Title
Hypothalamic hormone-sensitive lipase regulates appetite and energy homeostasis

Authors
Hundahl, Cecilie
Kotzbeck, Petra
Burm, Hayley B
et al.

Publication Date
2021-05-01

DOI
10.1016/j.molmet.2021.101174

Peer reviewed

Original Article

MOLECULAR METABOLISM

Hypothalamic hormone-sensitive lipase regulates appetite and energy homeostasis

Cecilie Hundahl [1,5], Petra Kotzbeck [2,8], Hayley B. Burm [1,5], Søren H. Christiansen [3], Lola Torz [1], Aske W. Helge [1], Martin P. Madsen [1], Cecilia Ratner [1,5], Annette K. Serup [4], Jonatan J. Thompson [5], Thomas O. Eichmann [2,6], Tune H. Pers [5], David P.D. Woldbye [3], Daniele Piomelli [6,7], Bente Kiens [4], Rudolf Zechner [2], Louise J. Skov [1,5,**], Birgitte Holst [1,5,*]

ABSTRACT

Objective: The goal of this study was to investigate the importance of central hormone-sensitive lipase (HSL) expression in the regulation of food intake and body weight in mice to clarify whether intracellular lipolysis in the mammalian hypothalamus plays a role in regulating appetite.
Methods: Using pharmacological and genetic approaches, we investigated the role of HSL in the rodent brain in the regulation of feeding and energy homeostasis under basal conditions during acute stress and high-fat diet feeding.
Results: We found that HSL, a key enzyme in the catabolism of cellular lipid stores, is expressed in the appetite-regulating centers in the hypothalamus and is activated by acute stress through a mechanism similar to that observed in adipose tissue and skeletal muscle. Inhibition of HSL in rodent models by a synthetic ligand, global knockout, or brain-specific deletion of HSL prevents a decrease in food intake normally seen in response to acute stress and is associated with the increased expression of orexigenic peptides neuropeptide Y (NPY) and agouti-related peptide (AgRP). Increased food intake can be reversed by adeno-associated virus-mediated reintroduction of HSL in neurons of the mediobasal hypothalamus. Importantly, metabolic stress induced by a high-fat diet also enhances the hyperphagic phenotype of HSL-deficient mice. Specific deletion of HSL in the ventromedial hypothalamic nucleus (VMH) or AgRP neurons reveals that HSL in the VMH plays a role in both acute stress-induced food intake and high-fat diet-induced obesity.
Conclusions: Our results indicate that HSL activity in the mediobasal hypothalamus is involved in the acute reduction in food intake during the acute stress response and sensing of a high-fat diet.

Keywords Appetite regulation; Stress; Obesity; Hypothalamus

1. INTRODUCTION

The global prevalence of obesity and metabolic comorbidities is increasing at an alarming rate and is further intensified by the lack of effective prevention measures and treatments. A sedentary lifestyle and high-energy food intake together with genetic predisposition are thought to be the main drivers of the development of obesity. However, maladaptation to stress may also play a role in the pathogenesis of obesity [1]. Considerable efforts are underway to reveal how the central nervous system senses and integrates hormonal and nutrient signals from the periphery to control energy homeostasis in response to environmental demands [2]. Substantial evidence suggests that regulation of lipid metabolism in the hypothalamus may contribute to this equilibrium [3,4] by regulating energy intake in accordance with energy availability [5,6]. Notably, long-chain fatty acids have been shown to modulate appetite [7,8], and central administration of fatty acids suppresses food intake and decreases hypothalamic expression of orexigenic neuropeptides agouti-related peptide (AgRP) and neuropeptide Y (NPY) [4,9]. However, it is unclear whether fatty acids and other lipid metabolites act locally after they are mobilized from lipid stores or whether circulating lipid species derived from dietary fat can act as a signal of energy surplus, thereby decreasing appetite [8].
In the post-prandial state, circulating fatty acids derived from dietary sources are transported in an esterified form as triacylglycerols in lipoproteins. Prior to fatty acid uptake by target tissues, lipoprotein lipase (LPL) releases fatty acids from lipoprotein-associated triacylglycerols. The role of these circulating fatty acids in the hypothalamic control of energy homeostasis has been evaluated by studying the effects of LPL deficiency in neurons [10–13] and astrocytes [14] in mice. While results varied, all the studies identified a weight gain in

[1]Department of Biomedical Sciences, University of Copenhagen, 2200 Copenhagen N, Denmark [2]Institute of Molecular Biosciences, University of Graz, Graz, Austria [3]Department of Neuroscience, University of Copenhagen, 2200 Copenhagen N, Denmark [4]Department of Nutrition, Exercise and Sports, University of Copenhagen, 2100 Copenhagen Ø, Denmark [5]Novo Nordisk Foundation Center for Basic Metabolic Research, University of Copenhagen, 2200 Copenhagen N, Denmark [6]Center for Explorative Lipidomics, BioTechMed-Graz, Graz, Austria [7]Department of Anatomy and Neurobiology, University of California, Irvine, CA, USA [8]Division of Endocrinology and Diabetology, Medical University of Graz, Graz, Austria

*Corresponding author. Department of Biomedical Sciences, University of Copenhagen, 2200 Copenhagen N, Denmark. E-mail: holst@sund.ku.dk (B. Holst).

**Corresponding author. Department of Biomedical Sciences, University of Copenhagen, 2200 Copenhagen N, Denmark.

Received December 11, 2020 • Revision received January 22, 2021 • Accepted January 25, 2021 • Available online 5 February 2021

https://doi.org/10.1016/j.molmet.2021.101174

mice lacking centrally expressed LPL. This finding was primarily ascribed to decreased locomotor activity and energy expenditure, with some effect on feeding [10–14]. However, the contribution of LPL-derived fatty acids cannot sufficiently account for the ability of the central administration of fatty acids to suppress food intake [4,9], suggesting that other sources of fatty acids, such as those released from intracellular triglyceride depots, may be more important for appetite control.

Intracellular fatty acids primarily originate from the hydrolysis of triacylglycerols located in cytoplasmic lipid droplets or from endocytosed lipoprotein-associated triacylglycerols [15]. Cytoplasmic lipolysis consists of three consecutive enzymatic reactions catalyzed by adipose triglyceride lipase (ATGL), hormone-sensitive lipase (HSL), and monoacylglycerol lipase (MGL) to release fatty acids from triacylglycerols, diacylglycerols, and monoacylglycerols, respectively. The process is tightly controlled by regulatory proteins and hormones [16,17] and occurs in many different tissues and cell types. In adipocytes, catecholamines released during acute stress or fasting activate ATGL and HSL, causing increased triacylglycerol hydrolysis and the release of fatty acids into the circulation [16]. Most other non-adipose cells utilize lipolysis-derived fatty acids endogenously as substrates for anabolic processes or oxidation [18].

HSL has been shown to be expressed and enzymatically active in the brain [19]. However, the functional role of this enzyme in the brain remains unexplored. Given the well-defined role of hypothalamic lipid sensing in the regulation of food intake, we hypothesize that HSL may contribute to intracellular sensing and signaling, thereby influencing hypothalamic regulation of appetite. To test this hypothesis, we investigated the role of rodent brain HSL in the regulation of feeding and energy homeostasis using a combination of pharmacological and genetic approaches.

2. METHODS

2.1. Animal studies

All the animal studies were carried out at the Rodent Metabolic Phenotyping Center at the Panum Institute in Copenhagen, Denmark. The animal studies were conducted in accordance with institutional, national, and European guidelines and approved by the Danish Animal Experiments Inspectorate (license numbers 2012-15-2934-00054 or 2014-15-0201-00181).

The animals had ad libitum access to water and a chow diet (Altromin #1314, Brogaarden, Denmark) unless otherwise stated. All the animals were housed in a temperature-controlled environment under a 12/12-h light–dark cycle. For ex vivo analysis of HSL expression and phosphorylation, C57BL/6 J mice (Janvier, Denmark) were used. Sprague Dawley rats (Taconic, Denmark) weighing 250 g at the time of surgery were used for the central inhibition of HSL.

2.1.1. Global HSL KO mice

For in vivo studies, the HSL knockout (KO) mice were generated by targeted disruption of the HSL gene as previously described [20,21]. Male HSL KO mice and age-matched WT littermates with a C57BL/6 background were obtained from heterozygous breeding and used for experiments at 16–26 weeks of age.

2.1.2. Brain-specific HSL KO mice

A mouse line fully backcrossed to a C57BL/6J background carrying a mutated *Lipe (HSL)* allele in which exons 2 to 7 were flanked by LoxP sites [19] was crossed with a C57BL/6J line expressing Cre recombinase under control of the Nestin promoter [22] (#003771, Jackson Laboratory, USA). As Nestin-Cre mice are known to have a phenotype characterized by low body weight and length [23], Cre-positive mice had to be used as controls. Thus, littermate controls were generated by crossing $HSL^{wt/fl}$;$cre^{-/-}$ females and $HSL^{wt/fl}$;$cre^{+/-}$ males, generating several genotypes, including the experimental groups: $HSL^{wt/wt}$;$cre^{+/-}$ (controls) and $HSL^{fl/fl}$;$cre^{+/-}$ (HSL^{brain}KO). Male mice were used in all the studies.

2.1.3. Sf1-specific HSL KO mice

Sf1 neuron-specific HSL-depleted (HSL^{Sf1}KO) mice were generated by crossing mice in which exons 2 to 7 in the HSL (*Lipe*) gene were flanked by LoxP sites [19] with mice expressing Cre recombinase under the control of the SF1 (mouse gene name, *Nr5a1*) promoter (#012462, Jackson Laboratory), resulting in a mixed C57BL/6J and FVB/NJ strain. Male mice were used in all the experiments.

The Sf1-specific deletion of HSL in the HSL^{Sf1}KO mice was verified by crossing the HSL^{Sf1}KO mice that had a loxP-flanked STOP cassette preventing transcription of a red fluorescent protein, TdTomato (#007908, Jackson Laboratory). Hypothalamic cells were isolated from 3-day-old pups using the Papain Dissociation System (Worthington Biochemical Corp., USA), allowing fluorescence-activated cell sorting (FACS) of Cre-expressing $Sf1^{+}$-cells, as TdTomato is expressed only in Cre-expressing cells. Following FACS, the expression of a reference gene (*Ywhaz*) and HSL (*Lipe*) was verified by qPCR, and the PCR product was run on an agarose gel.

2.1.4. AgRP-specific HSL KO mice

AgRP neuron-specific HSL-depleted mice were generated by crossing C57BL/6J mice in which exons 2 to 7 in the HSL (*Lipe*) gene were flanked by LoxP sites [19] with mice expressing Cre recombinase under the control of the AgRP promoter (#012899, Jackson Laboratory) that were backcrossed for five generations to a C57BL/6J background. Male mice were used in all the experiments.

2.1.5. Virus constructs

For hypothalamic HSL overexpression, a recombinant adeno-associated virus (rAAV) vector was used. The vector was a chimeric serotype consisting of capsids from serotype 1 and inverted terminal repeats from serotype 2. The transgenes were subcloned into an expression cassette containing a hybrid promoter consisting of a CMV enhancer and a human synapsin I promoter fragment, woodchuck post-transcriptional regulatory element, and a bovine growth hormone polyA signal flanked by viral inverted terminal repeats. The rAAV vectors were manufactured by Vector Biolabs (USA) and encoded the full-length cDNA for mouse HSL (RefSeq: BC021642; titer: 2.5×10^{13} genomic particles/ml) or a control empty cassette vector containing only a GFP sequence (titer: 6.0×10^{13} genomic particles/ml).

2.1.5.1. Adeno-associated virus vector delivery of HSL gene in the mediobasal hypothalamus. The animals were anesthetized by inhalation of 4% isoflurane (Baxter Medical AB, Sweden) at 0.4 L/min and fixed in a stereotaxic frame (Kopf Instruments, USA). Before the surgery, the mice received 5 mg/kg of Rimadyl (Pfizer, USA) s.c. and a drop of 10 mg/ml of lidocaine (Farmaplus, Norway) in the incision. A volume of 1 μl of viral vector suspension was infused through a glass pipette (0.1 μl/min) bilaterally into the VMH (anterior-posterior (AP) −1.6 mm, medial-lateral (ML) ± 0.5 mm, and dorsal-ventral (DV) −5.6 mm) [24]. Reference points were the bregma for the AP axis, midline for the ML axis, and the skull for the DV axis. The pipette was left in place for an additional 3 min after infusion to prevent backflow of viral particles through the injection track. The mice were treated post-operatively with 5 mg/kg of Rimadyl (Pfizer) s.c. for three days.

To verify the location of virus delivery into the mediobasal hypothalamus, a separate small cohort of mice were infused with the control empty cassette vector containing only GFP (6.0×10^{13} genomic particles/ml). The same coordinates and procedure as previously described were used. Three weeks after surgery, the mice were anesthetized with pentobarbital (75 mg/kg) i.p. and transcardially perfused with 0.9% saline for 3 min, followed by 4% paraformaldehyde (Sigma–Aldrich, Denmark) for 5 min. Whole brains were post-fixed in 4% paraformaldehyde overnight and cryoprotected in 30% sucrose in phosphate-buffered saline (PBS) for 3 days. Coronal sections (20 μm) spanning the entire hypothalamus were collected using a cryostat and mounted on Superfrost Plus slides (Thermo Fisher Scientific, USA).

Hypothalamic sections were blocked (2% BSA and 0.1% Triton X in 0.01 M of PBS) for 45 min. The sections were incubated overnight with primary antibody (chicken anti-GFP antibody, 1:2000, Aves Labs, USA) and subsequently for 2 h with secondary antibody (Alexa Fluor anti-chicken 488, 1:200, Thermo Fisher Scientific).

2.1.6. HSL inhibitor and isoproterenol ICV administration

The rats were anesthetized with 0.27 ml/kg of Hypnorm/Midazolam (fentanyl citrate, 0.07875 mg/ml; fluanisone, 2.5 mg/ml; and midazolam, 1.25 mg/ml), while the mice were anesthetized with 4% isoflurane at 0.4 L/min. All the rodents were administered 5 mg/kg of Rimadyl (Pfizer) s.c. before and three days after surgery and a drop of 10 mg/ml of lidocaine (Farmaplus) and a drop of 5 mg/ml of marcaine (AstraZeneca, Denmark) were applied locally. In a stereotaxic frame, a sagittal incision was made along the scalp and the bone suture junctions were used as reference points for cannula placement. In relation to the bregma, the brain cannulas were positioned in the rats (AP: −1.0 mm and ML: 1.5 mm) and mice (AP: −0.3 mm and ML: 1.0 mm). The cannulas were secured using 1.0 mm stainless steel anchor screws (AgnTho's, Sweden) and dental cement (Poly-F Plus, Dentsply, Denmark) in the rats, while cannulas were secured with only dental cement in the mice. To test the cannula placement, the rodents received an intra-cerebroventricular (ICV) administration of 100 ng of human angiotensin II (Sigma–Aldrich) with a handheld 10 μl syringe (Hamilton 1701RN, AgnTho's). Only the rodents that showed an immediate increase in water intake after angiotensin II administration were included in the studies.

ICV administration of the HSL inhibitor NNC76-79 (NNC 0076-0000-0079 provided by Novo Nordisk, Denmark, 5 μl of 50 μM in 100% DMSO) into the cohort of rats was performed over 2 h, ranging from 1 to 3 h before the dark phase, but an effect was seen only after initiation of the dark phase and food intake during the first 40 min of the dark phase. The compounds were infused slowly over a 1-min period and the injector needle was left in place for 30 s after each infusion to prevent backflow. Food intake was recorded using MANI FeedWin cages (Ellegaard Systems, Denmark). To ensure that the rats did not transport food from the food hoppers into the cage, they were offered powdered Altromin chow (Brogaarden).

ICV administration of either isoproterenol (1 μl of 100 nM in 100% DMSO, Sigma–Aldrich) or 100% DMSO was performed in the HSL KO and control mice just before the dark phase as previously described. Metabolic parameters and food intake were recorded using an indirect calorimetry system (PhenoMaster, TSE Systems, Germany) immediately after the administration.

2.1.7. Metabolic phenotyping

Body weight was measured and fat and lean mass of the unanesthetized mice was assessed by quantitative magnetic resonance imaging (MRI) using EchoMRI (Echo Medical Systems, USA). Diet-induced obese mice were fed a high-fat diet (HFD) with 45 kcal% fat (D12451, Research Diets, Brogaarden). Food intake was assessed manually for the entire period. Automated measurement of mouse food intake, energy expenditure, and spontaneous home cage activity was performed in an indirect calorimetry system (PhenoMaster, TSE Systems). The mice were allowed to acclimatize to the system for a minimum of 3 days unless they were subjected to novelty stress.

For fasting experiments, the mice were fasted for 24 h with free access to water starting in the beginning of the dark phase. Injection stress was induced just before the dark phase by scruffing the mouse and injecting 5 ml/kg of saline s.c. in the inguinal area. Unless otherwise stated, food intake during the following 2 h is shown.

To induce novelty stress, the mice were moved from being group housed to being single housed in a new cage in the TSE system, with a different size than their home cage and new food and water containers. The move was done just before the beginning of the dark phase.

For restraint stress, the mice were placed in 50 ml NUNC tubes for 30 min and then placed back in their home cage at the beginning of the dark phase.

Predator stress was simulated by exposing the mice to a cotton swap with water or a 1:1000 dilution of 2,4,5-trimethylthiazoline (a constituent of fox urine and feces that is proposed to be an innately aversive odor to rodents) in their home cage during the last 30 min before the dark phase.

Glucose tolerance was assessed in a separate cohort of 10 $HSL^{Sf1}KO$ mice and 10 littermate controls that had been fed a high-fat diet for 12 weeks. The mice were fasted for 16 h with free access to water. Glucose (2 g/kg body weight) was administered by oral gavage. The blood glucose concentration was measured using a glucometer (Ascensia Elite XL diabetes care system, Bayer Healthcare, Germany) at 0, 15, 30, 60, and 120 min time points. At 0 and 15 min time points, blood was collected from the orbital sinus, and plasma was used for measuring insulin using a Mouse/Rat Insulin kit (K152BZC, Meso Scale Discovery, USA) according to the instructions provided.

2.2. In situ hybridization

The procedure was performed as previously described, with minor modifications [25,26]. The mice were euthanized by decapitation, and their brains were quickly removed, frozen on dry ice, and cut into 15-μm coronal serial sections onto Superfrost Plus glass slides and stored at −80 °C until further processing. The slides were defrosted for 10 min at room temperature (RT), fixed in 4% paraformaldehyde for 5 min, and rinsed in PBS for 2 × 5 min. The slides were then acetylated for 10 min (0.25% acetic anhydride, 0.9% NaCl, and 1.4% triethanolamine), run through a series of washing steps (70% ethanol for 5 min, 95% ethanol for 1 min, 99% ethanol for 1 min, chloroform for 5 min, 99% ethanol for 1 min, and 95% ethanol for 1 min), and left to dry. The following synthetic anti-sense oligonucleotide DNA probe was used: HSL mRNA: 5-AAA ATG GTC CTC TGC CTC TGT CCC TGA ATA GGC ACT GAC ACA CTT-3. The oligoprobe was labeled at the 3 end with [^{33}P]dATP (3000 Ci/mmol, NEG312H250UC, PerkinElmer, Denmark) using terminal deoxynucleotidyl transferase (Roche Diagnostics, Germany). The labeled probe was added to a hybridization buffer (50% formamide (v/v), 20% saline sodium citrate (x20), 10% dextran sulphate, 2% Denhardt's (x50), 0.5% yeast t-RNA (50 mg/ml), 5% salmon DNA sperm (10 mg/ml), and 10 mM of dithiothreitol. After adding a volume of 120 μl of hybridization mixture to each slide, the slides were covered with parafilm and left at 37 °C in humidity boxes overnight. At RT, the slides were subsequently briefly rinsed in 1x saline sodium citrate, washed for 4 × 15 min in 1x saline sodium

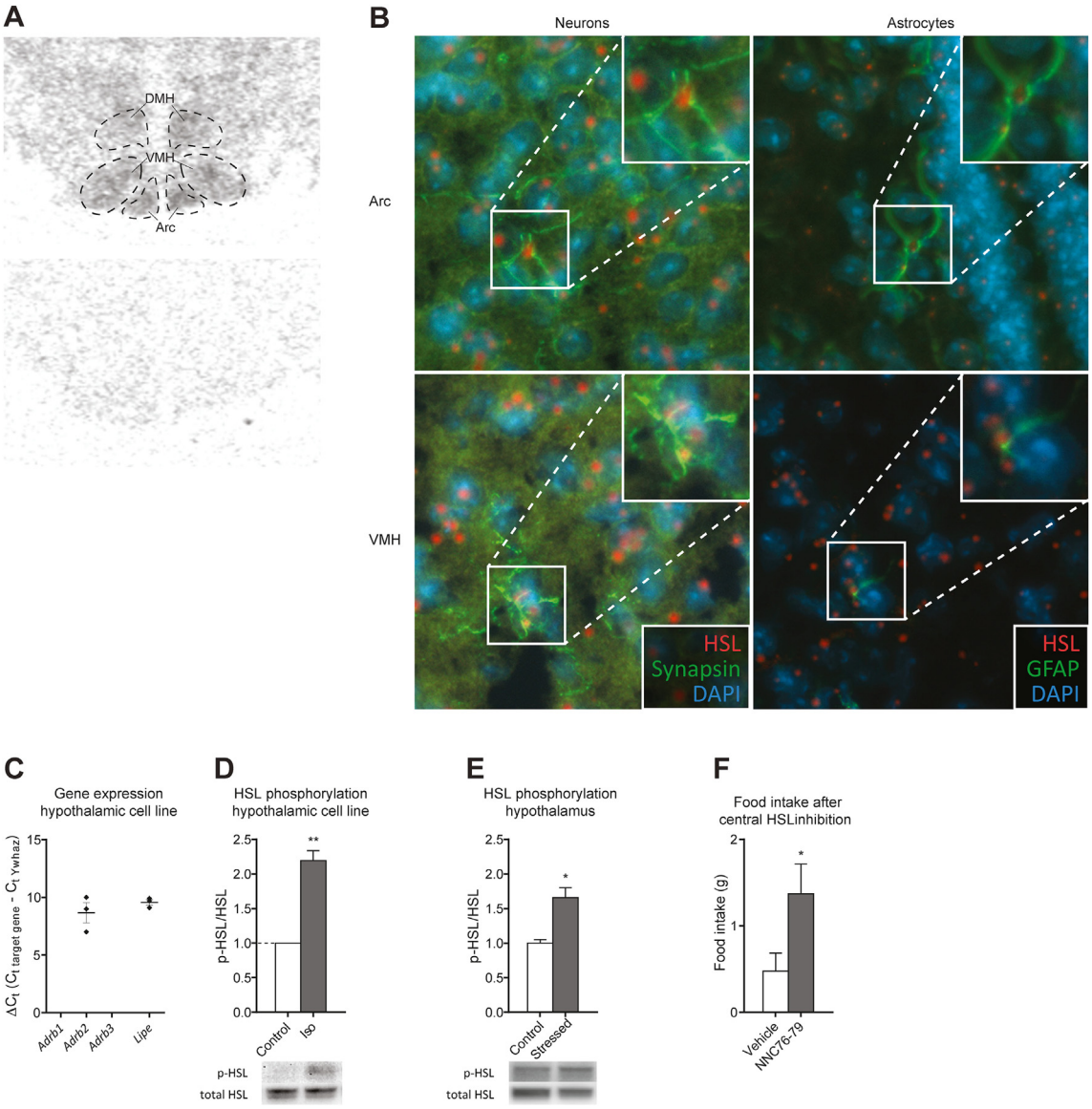

Figure 1: HSL expression and regulation in the hypothalamus. A) In situ hybridization showing HSL expression (top) located primarily in hypothalamic nuclei involved in appetite regulation, namely the dorsomedial (DMH), arcuate (Arc), and ventromedial (VMH) nuclei and non-specific binding (bottom). B) RNAscope/immunohistochemistry showing HSL mRNA transcripts (red) in neurons and astrocytes (green) in Arc and VMH. C) Gene expression of β-adrenergic receptors (*Adrb1-3*) and HSL (*Lipe*) in a hypothalamic cell line and D) HSL activation (phosphorylation) at S660 after treatment with isoproterenol in the same cell line ($n = 3$ for each separate experiment and data were normalized so the p-HSL/HSL value was 1 for the controls) and E) in vivo after injection stress ($n = 3$) in C57bl/6J mice. F) Food intake in Sprague Dawley rats 1 h after central administration of an HSL inhibitor ($n = 8$). Data are mean ± SEM. *$p < 0.05$ and **$p < 0.01$ based on Student's unpaired t test.

citrate at 60 °C, and passed through a series of 1 min rinses in 1x saline sodium citrate, 70% ethanol, and 95% ethanol. The slides were air-dried and exposed together with ^{14}C microscales to ^{33}P-sensitive Kodak BioMax MR films (Amersham Biosciences, Denmark) for 2–4 weeks and developed in Kodak GBX developer.

2.3. RNAscope/immunohistochemistry

For the localization of hypothalamic HSL, brains from the sacrificed mice were coronally cryosectioned, fixed in a 10% formalin solution for 1 h, and dehydrated and stored in 100% ethanol. To detect HSL mRNA, a commercially available branched chain in situ hybridization kit (RNAscope, Advanced Cell Diagnostics, USA) was used according to the standard protocol provided. Following RNAscope, the sections were blocked with BSA and incubated with primary antibody (1:5000 for anti-GFAP and 1:1000 for anti-synapsin) and secondary antibody (Alexa Fluor, Thermo Fisher Scientific, 1:200) and mounted with Prolong Gold Antifade with DAPI.

2.4. Single-cell analysis

The Drop-seq protocol [27] mouse hypothalamic arcuate-median eminence complex single-cell RNA dataset published by Campbell et al. [28] was used to quantify the relative abundances of lipase transcripts within different populations of the arcuate nucleus (Arc) of the hypothalamus. The raw data and metadata with cell cluster annotations containing a total of 20,921 cells was downloaded from the Gene Expression Omnibus database (GSE93374). The single-cell analysis was performed using Seurat R packages (version 3.0) [29] unless otherwise specified.

The cell cluster plot in Suppl. Figure 1 was produced as follows. The raw unique molecular identifier (UMI) data were normalized using the NormalizeData command with default parameters, whereby each UMI count was divided by the total within the cell multiplied by a common scaling factor of 1e4, inflated by a single pseudocount (to avoid zeros), and transformed by the natural logarithm. The command FindVariableFeatures was used to identify 2,000 variable genes (the default) using the "vst" method. The variable genes were scaled using the ScaleData command, regressing out "percent.mito," "percent.ribo," and "nCount_RNA" using the default linear model. The RunPCA command was used to compute the first 40 principal components. The RunTSNE command was used to compute a t-distributed Stochastic Neighbor Embedding (t-SNE), with the "tsne.method" set to "Rtsne" using the first 30 pca dimensions and a perplexity of 30 with the additional argument check_duplicates = F. For the RunPCA and RunTSNE commands, the seed use argument was 12,345. The FeaturePlot command was then used to produce a t-SNE plot showing the expression of *Lipe* on a LogNormalized scale (Figure 1C, cell cluster plot).

The mean number of *Lipe* transcripts within each major cell population (Figure 1C, bar plot) and mean transcripts of different lipases in hypothalamic Arc neurons (Supp. Figure 1, bar plot) were computed by grouping cells labeled by Campbell et al. as neurons ("a13," "a14," "a15," "a16," "a17," and "a18"), oligodendrocytes ("a01," "a02," and "a05"), oligodendrocyte precursor cells ("a06"), astrocytes ("a10"), and tanycytes ("a11" and "a12"), respectively, under these coarser labels. The mean transcript counts and errors were computed by fitting a negative binomial distribution to the UMI counts with the fitdistr function from the MASS R package [30]. The data were plotted with ggplot, geom_col, and geom_errorbar functions from the ggplot2 R package [31]. The code to reconstruct Figure 1C can be found at https://github.com/perslab/hundahl-2019.

2.5. Hypothalamic cell line

For the in vitro assessment of HSL phosphorylation, an NPY-expressing hypothalamic cell line (CLU499, Cellutions Biosystems, Canada) was used and maintained as previously published32.

2.6. Western blotting

The mice were euthanized by decapitation and their brains quickly dissected. The hypothalamus was scooped out, snap-frozen in liquid nitrogen, and stored at −80 °C until further use as described as follows. To detect total HSL, m. gastrocnemius muscle and a portion of subcutaneous adipose tissue were also dissected. Hypothalamic cells (CLU499, CELLutions Biosystems) were serum-fasted for 2 h and then treated with 1 μM of isoproterenol (Sigma–Aldrich) for 15 min. The samples were lysed in 0.4 mL of RIPA lysis buffer (Millipore, Denmark) containing protease inhibitor cocktail cOmplete mini (Roche, Denmark) and phosphatase inhibitors (Sigma, Denmark), homogenized for 1 min at 50 Hz, and debris was cleared by centrifugation at 10,000 *g* at 4 °C for 15 min. The supernatant was collected, and the protein concentration was determined with a BCA kit (Thermo Fisher Scientific, Denmark). Equal amounts of protein per well were diluted in NuPage LDS 4x sample buffer (Invitrogen, Denmark) containing 1/5 0.1 M of DTT and heated to 92 °C for 5 min. Protein extracts were separated on 4–10% SDS-PAGE gels (Novex, Denmark) in SDS running buffer (Invitrogen) with 500 μl of NuPAGE antioxidant (Invitrogen). Proteins were transferred from the gels to PDVF transfer membranes (Thermo Fisher Scientific) by semi-dry blotting in NuPAGE transfer buffer (Novex) at 25 V for 1.5 h. The membranes were blocked for 1 h using StartingBlock T20 (TBS) Blocking Buffer (Thermo Fisher Scientific) and incubated with primary antibody (HSL, #4107, 1:1000, Cell Signaling, USA; p-HSL (S660), #4126, 1:1000, Cell Signaling) overnight at 4 °C. The membranes were washed 3 × 10 min in PBS with 0.1% Tween-20 before incubation for 2 h at RT with a horseradish peroxidase (HRP)-conjugated anti-rabbit secondary antibody (GE Healthcare, Denmark). The membranes were washed again, and bands were visualized by using Immobilon Western (Millipore). For studies with p-HSL, the membranes were then stripped using Restore Western Blotting Stripping Buffer (Thermo Fisher Scientific) and incubated overnight at 4 °C with total HSL antibody. For p-HSL, the bands were quantified by densitometry using AlphaView SA (ProteinSimple, USA) and the amount was compared to the amount of total HSL.

2.7. Laser capture

The Arc and VMH were collected bilaterally from 6 to 8 individual 14-μm coronal sections per animal on Superfrost Plus glass slides. Brain sections were stained for 1 min with 0.1% cresyl violet acetate (Sigma–Aldrich) dissolved in 70% ethanol. The sections were subsequently briefly dehydrated in 96% and 99.9% ethanol and then dried at RT for at least 2 min. Using a PALM Microdissection instrument (Zeiss Microsystems, Germany), the brain nuclei were identified and captured on CapSure Macro LCM Caps (Life Technologies, Applied Biosystems, USA).

2.8. qPCR

RNA was extracted from the microdissected Arc and VMH samples using an RNeasy Micro kit (Qiagen, Denmark) and the hypothalamus samples using an RNeasy Lipid Tissue Mini kit (Qiagen) according to the manufacturer's instructions. RNA was transcribed into cDNA using a SuperScript III Reverse Transcriptase kit (Invitrogen). KAPA SYBR FAST qPCR Master Mix (Kapa Biosystems, USA) was used for qPCR performed by LightCycler 480 (Roche). The program contained a pre-incubation step (95 °C for 30 s) and several amplification steps (45 cycles at 95 °C for 30 s and 60 °C for 60 s). Tyrosine 3-monooxygenase/tryptophan 5-monooxygenase activation protein zeta polypeptide (YWHAZ) was used for the hypothalamus samples, and TATA-binding protein (TBP) was used for normalization (see Table 1).

Table 1 — Primers used for qPCR.

Gene	Forward primer (5' → 3')	Reverse primer (5' → 3')
Acc	TCCTTGTGGATTACGGACTGCGAA	CCGGCTCCAAGTGGCGGTA
Acs	GAAGATCAAGCGAGGCTCCA	CCTTCCTGCATTCCATCGTC
Aif1	ATCAACAAGCAATTCCTCGATGA	CAGCATTCGCTTCAAGGACATA
Agrp	GCTGCAGAAGGCAGAAGC	GACTCGTGCAGCCTTACACA
Bsx	TTTCTGACTCGCAGCTCTCC	CTGGAACGTTTTCACCT
Cb1	TGCTTGCGATCATGGTGTAT	TGTCTCAGGTCCTTGCTCCT
Cpt1a	ATGTGGACCTGCATTCCTTC	GAACTTGCCCATGTCCTTGT
Cpt1c	AGAAGTAGACTCAGCTCG	CCAGAGATGCCTTTTCCAG
Fasn	CCCTTGATGAAGAGGGATCA	ACTCCACAGGTGGGAACAAG
Foxo	GCAACGCGTGGGGCAACCTGT	GGGCACGCTCTTCACCATCCACTC
Gfap	GTTTCATCTTGGAGCTTCTGC	GGAGGTGGAGAGGGACAAC
Ghsr	AAGATGCTTGCTGTGGTGGT	AAAGGACACCAGGTTGCAGT
Lipe	CCGTTCCTGCAGACTCTCTC	CCACGCAACTCTGGGTCTAT
Mgll	CAGAGAGGCCAACCTACTTTTC	ATGCGCCCCAAGGTCATATTT
Npy	TGGACTGACCCTCGCTCTAT	TGTCTCAGGGCTGGATCTCT
Npyy1r	CGGCGTTCAAGGACAAGTAT	CGTTGATTCGTTTGGTCTCA
Pnpla2	CACAGCGCTGGTCACTGGGG	CCGGGCCTCCTTGGACACCT
Pomc	AGAGAGCTGCCTTTCCGCGAC	GCAGGAGGGCCAGCAACAGG
Sirt1	CGCAGTCTCCAAGGAGCTCTACA	TGGATCTTCTCTGAAAGTGAGACCAGT
Tbp	TCAAACCCAGAATTGTTCTCC	GGTAGATGTTTTCAAATGCTTCA
Ucp2	CCTACAAGACCATTGCACGA	TGTCATGAGGTTGGCTTTCA
Ywhaz	AGACGGAAGGTGCTGAGAAA	GAAGCATTGGGGATCAAGAA

The threshold cycle (Ct) values were obtained by the instrument's software using the second derivative method. The expression of the gene of interest was normalized to the expression of the two housekeeping genes TBP and YWHAZ as a control for experimental variability using the ΔCt method. To check for primer-dimer artifacts and ensure the reaction's specificity, a post-amplification melting curve analysis was performed using LightCycler 480 software.

2.9. Plasma free fatty acid measurements

Eight HSL KO mice and 8 littermate controls were fasted for 24 h, and their blood was collected after termination. For quantitative determination of plasma free fatty acid levels, a NEFA-HR kit (Wako, USA) was used according to the manufacturer's instructions.

2.10. Acylated ghrelin measurements

To measure the amount of acylated ghrelin in plasma after a 24-h fast, an Acylated Ghrelin (mouse/rat) Enzyme Immunometric Assay kit (Bertin Pharma, France) was used according to the manufacturer's instructions. Fourteen wild-type and 13 global HSL knockout male mice were fasted for 24 h. To prevent degradation of the acylated ghrelin, blood was collected from the orbital sinus in tubes containing EDTA and treated with p-hydroxymercuribenzoic acid and HCl according to the kit's instructions.

2.11. Corticosterone measurements

Blood samples from 8 mice with each genotype (the $HSL^{Sf1}KO$ and control mice) were collected from the orbital sinus after injection stress and on a separate day as a control. A Mouse/Rat Corticosterone kit (#DEV9922, Demeditec Diagnostics, Germany) was used according to the manufacturer's instructions.

2.12. Lipid analysis

Plasma (70 μl) or hypothalamus explants (<15 mg) were extracted as described by Matyash et al. [33]. In brief, the samples were homogenized using two beads (6 mm stainless steel) on a Mixer Mill (Retsch, Germany; 2 × 10 s, frequency 30/s) in 700 μl of methyl-tert-butyl ether (MTBE)/methanol (3/1, v/v) containing 500 pmol of butylated hydroxytoluene, 1% acetic acid, and internal standards (IS; 1000 pmol of 17:0 fatty acid, 200 pmol of 17:0/17:0/17:0 triacylglycerol, and 67 pmol of 17:0_17:0 diacylglycerol, Larodan, Sweden). Total lipid extraction was performed under constant shaking for 30 min at RT. After adding 140 μl of dH2O (70 μl for the plasma samples) and further incubation for 30 min at RT, the samples were centrifuged at 1,000× g for 15 min. Then 500 μl of the upper organic phase was collected and dried under a stream of nitrogen. Lipids were resolved in 500 μl of MTBE/methanol (3/1, v/v) and diluted in 2-propanol/methanol/dH2O (7/2.5/1, v/v/v) for UHPLC-qTOF analysis. Then, 50 μl of each lipid extract was used for fatty acid derivatization using an AMP + MaxSpec kit (Cayman Chemical, USA) according to the manufacturer's protocol. Remaining proteins were solubilized in 0.3 N of NaOH at 65 °C for 4 h and the protein content was determined using Pierce BCA reagent (Thermo Fisher Scientific) and BSA as a standard.

Chromatographic separation was performed on a 1290 Infinity II LC system (Agilent, USA) equipped with a Luna Omega C18 column (2.1 × 50 mm, 1.6 μm, Phenomenex, USA) running a 20 min linear gradient from 55% solvent A (H2O; 10 mM of ammonium acetate, 0.1% formic acid, and 8 μM of phosphoric acid) to 100% solvent B (2-propanol; 10 mM of ammonium acetate, 0.1% formic acid, and 8 μM of phosphoric acid). The column compartment was kept at 50 °C. A 6560 Ion Mobility Q-TOF mass spectrometer (Agilent) equipped with Dual AJS ESI source was used to detect lipids in the positive Q-TOF mode. Data acquisition was performed by MassHunter Data Acquisition software (B.09, Agilent). The lipids were manually identified and lipid feature extraction was conducted using MassHunter Profinder (V.10, Agilent). Data were normalized for recovery, extraction, and ionization efficacy by calculating analyte/IS ratios (AU) expressed as AU/mg protein.

2.13. Quantification and statistical analysis

Statistical analysis was performed using Prism 7 (GraphPad, USA), and the data are presented as mean ± SEM. Probability values less than 0.05 were considered statistically significant. Student's t test was used to compare the means in two groups. Two-way repeated-measures analysis of variance followed by Šídák's multiple comparisons test or one-way analysis of variance followed by Tukey's multiple comparisons test were used as described in figure legends.

3. RESULTS

3.1. Hormone-sensitive lipase (HSL) was expressed and functionally active in the hypothalamus

To study the presence of HSL in different brain regions, we determined the HSL mRNA expression in the brain using in situ hybridization. This revealed that HSL was expressed in the entire brain (data not shown) with high levels in the hypothalamus and specifically the hypothalamic nuclei related to homeostatic feeding regulation, namely the Arc, ventromedial hypothalamic nucleus (VMH), and dorsomedial hypothalamic nucleus (DMH) (Figure 1A). We also demonstrated that HSL mRNA was expressed in both neurons and astrocytes in the Arc and VMH using RNAscope (Figure 1B). In the figure, each red dot represents one transcript of HSL mRNA, which was co-localized with the mRNA of synapsin and glial fibrillary acidic protein (GFAP), respectively. This was in accordance with a dataset published by Campbell et al. [28] (GEO accession number GSE93374), where single-cell transcriptomics of cells from the Arc confirmed that HSL was expressed in neurons in addition to all of the other cell types (Supp. Figure 1A). Other lipases involved in intracellular degradation of triacylglycerols such as MGL and ATGL were also expressed in Arc neurons (Supp. Figure 1B). However, we chose to focus our current studies on HSL due to its well-described regulation in the periphery.

To evaluate whether HSL could be activated in the hypothalamus, we measured the phosphorylation of HSL both in a hypothalamic cell line and the hypothalamus of the mice. The cell line was derived from NPY-expressing hypothalamic neurons (mHypoA-NPY) [32] and expressed both HSL (*Lipe*) and the β_2-adrenergic receptor (*Adrb2*), but none of the other β-adrenergic receptors (Figure 1C). Since acute stress activates HSL in the peripheral tissues via β-adrenergic signaling, we measured the phosphorylation of HSL^{660} following treatment with a β-adrenergic agonist isoproterenol in vitro using this cell line [16]. Treatment with isoproterenol resulted in increased HSL^{660} phosphorylation (Figure 1D), which was the PKA regulatory site. A similar increase in phosphorylation of HSL^{660} in the hypothalamus was observed in vivo when the mice were exposed to an acute stressful intervention by injection (Figure 1E), suggesting that HSL in the hypothalamus may be activated via the canonical β-adrenergic/cAMP/PKA pathway.

To test for the functional role of HSL in the hypothalamus, we blocked the enzymatic activity of HSL by administering a specific pharmacological inhibitor (NNC-76-70) via ICV injection in ad libitum fed rats. We found that acute suppression of HSL activity increased food intake (Figure 1F), suggesting that basal HSL activity suppresses appetite.

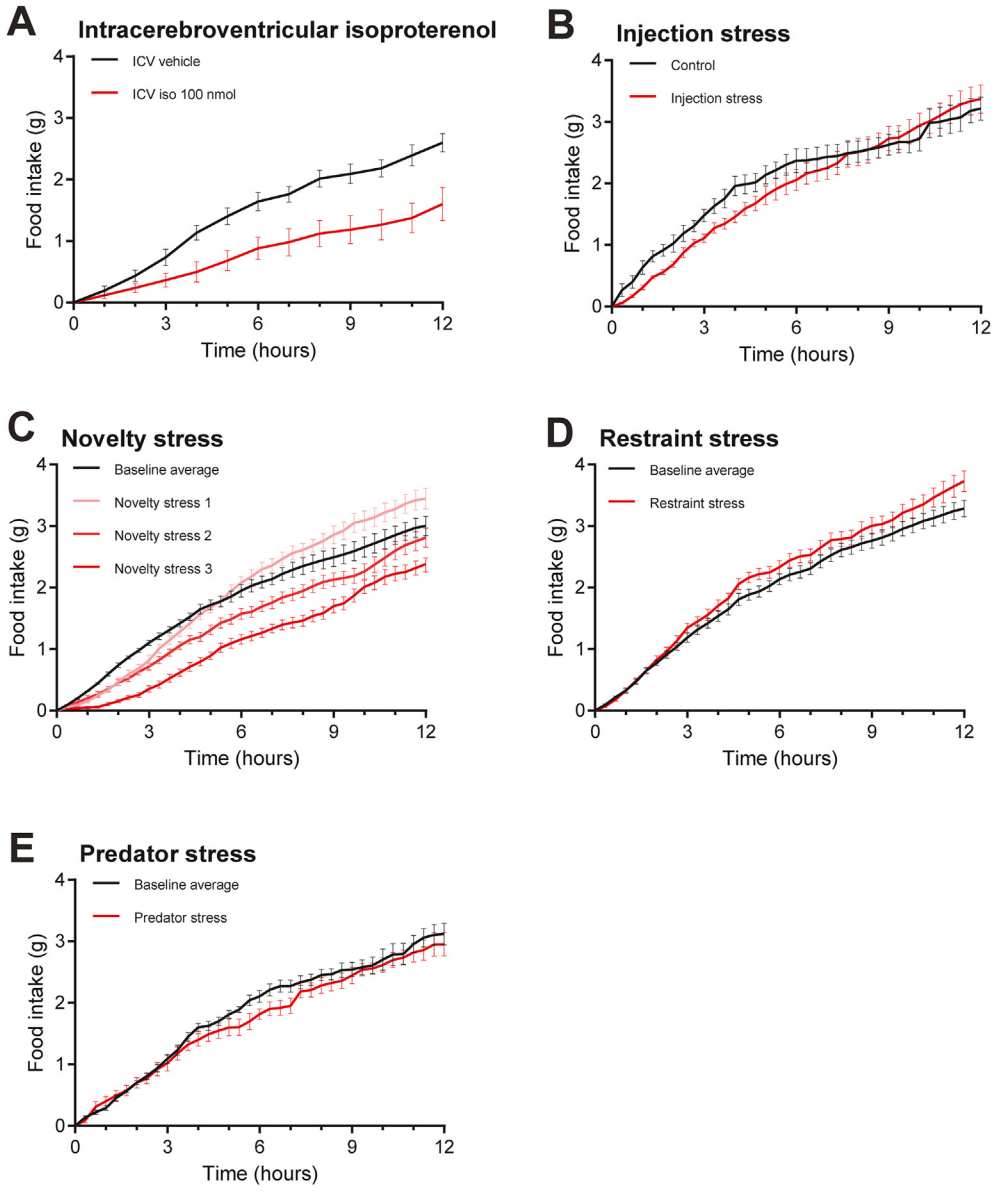

Figure 2: The effect of acute stress models on food intake. A) Food intake after ICV administration of 100 nmol isoproterenol or vehicle (n = 12). B) Food intake in mice stressed with an injection of saline and non-stressed controls (n = 8). C) Food intake after transferring the mice to new type of cage (novelty stress 1), a new cage without nesting material (novelty stress 2), and a new cage with no bedding at all (novelty stress 3) (n = 16) compared to the baseline average (the baseline average was calculated for each cohort, resulting in n = 3). D) Food intake after 30 min of restraint stress compared to the baseline average of the same cohort of mice (n = 16). E) Food intake after 30 min of exposure to a cotton swab with water or a 1:1000 dilution of 2,4,5-trimethylthiazoline (n = 8). Data are mean ± SEM.

3.2. Evaluation of acute stress models that affect food intake

As β-adrenergic signaling and acute stress activated HSL in the hypothalamus [34] and central inhibition of HSL increased food intake in the rats, we hypothesized that HSL plays a role in regulating food intake during the acute stress response.

To test the hypothesis that central HSL plays a role in stress-induced hypophagia, we required a robust and valid model of how acute stress affects food intake. Previous studies have shown that depending on the type of stress and experimental settings, stress may increase or reduce food intake [35]. However, most animal studies showed that acute stress causes reduced food intake [35–38]. To find a model in which there is an acute decrease in food intake and minimal harm to the mice, we tested several known models of acute stress in C57bl/6 mice.

First, we used isoproterenol injected ICV to test how a pharmacological imitation of the β-adrenergic stress response affects food intake. ICV isoproterenol administration decreased food intake by approximately 40% after 12 h compared to vehicle-treated controls (Figure 2A).

Despite their use in routine laboratory procedures, subcutaneous injections cause a mild acute stress response in mice [39] and accordingly affect food intake. Thus, we tested the effect on subsequent food intake after a single subcutaneous injection of saline compared to control mice that were not handled and found that injection stress decreased food intake by 33% 2 h after the injection (Figure 2B).

Exposure to a new environment is known to attenuate food intake in mice [40]. We exposed three separate cohorts of mice to different

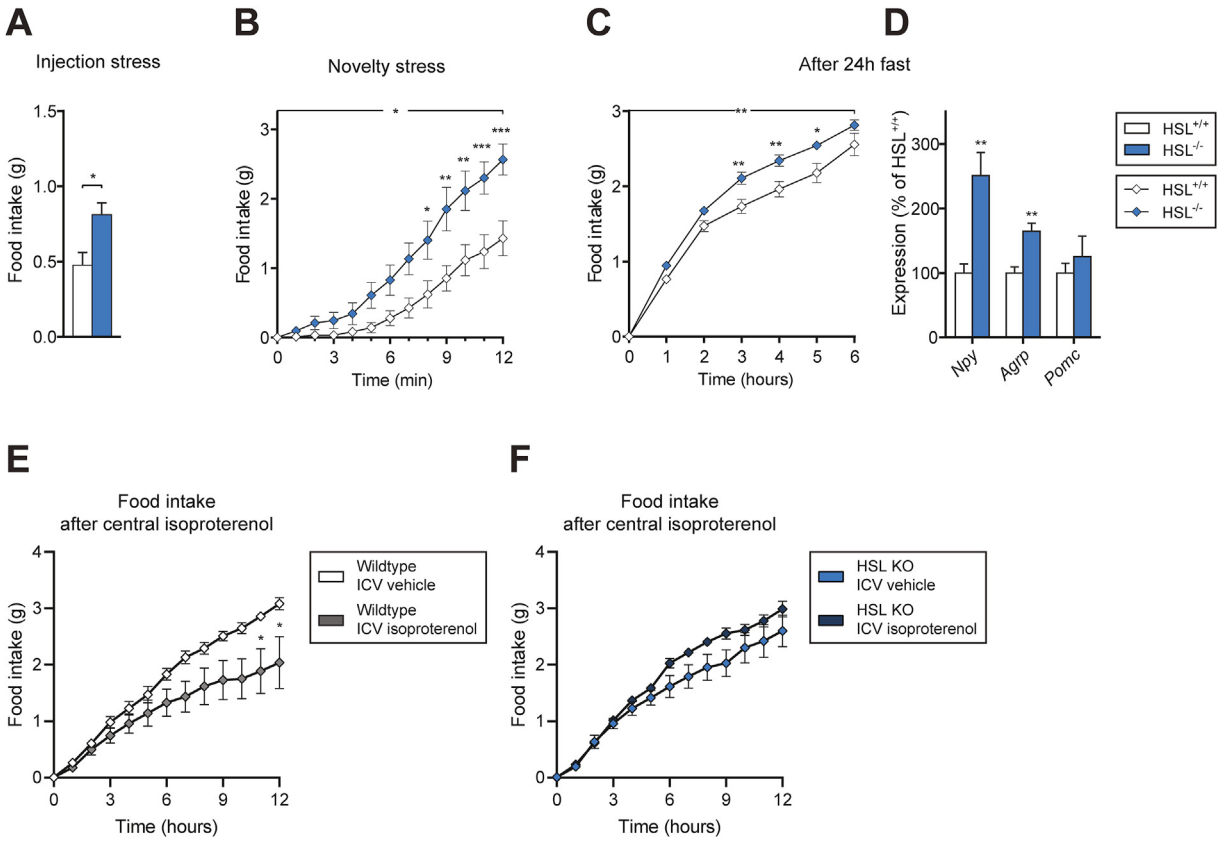

Figure 3: Appetite phenotype in global HSL KO and littermate control mice. A) Food intake in the mice following transfer to a novel environment (n = 8). B) Food intake 2 h after injection stress (n = 12). C) Food intake and D) gene expression of hypothalamic neuropeptides involved in appetite regulation after 24 h of fasting (n = 8). E) Food intake following ICV injection of 100 nmol of isoproterenol in wild-type mice (n = 7) and F) HSL KO mice (n = 7). Data are mean ± SEM. *p < 0.05, **p < 0.01, and ***p < 0.001 based on Student's unpaired t test (A and D) or repeated-measures two-way analysis of variance followed by Šídák's multiple comparisons test (B, C, E, and F).

housing conditions and compared the effects of each condition on food intake relative to their average baseline food intake (Figure 2C). The first cohort was monitored after being put into a new but normal cage. In this setup, the mice initially ate less (novelty stress 1), but during the night over-compensated and ate more than the baseline average. The second group was put into a cage containing only bedding material with no enrichment (novelty stress 2), and the third into a totally empty plastic cage (novelty stress 3). In these two groups, the food intake was more significantly reduced for a longer time period.

Restraint stress has been shown to decrease food intake and locomotor activity [41]. In this case, we restrained the mice for 30 min in a 50 ml conical tube, but this treatment did not result in any changes in the subsequent food intake (Figure 2D). The restraint stress was repeated for two more days, but the result was the same.

2,4,5-Ttrimethylthiazoline is a fox feces odor frequently used to elicit fear-induced behaviors [42]; hence, we tested whether its presence impacted food intake in the mice. However, this odor's presence had no effect on food intake (Figure 2E), and in our hands, the mice did not show any signs of fear.

In summary, the least harmful stress model for the mice that resulted in a decrease in food intake was exposure to injection stress, which decreased food intake by 33% after 2 h. Thus, this model was used in subsequent studies, and in all of the cases, food intake for 2 h after stress exposure was analyzed. In addition, novelty stress 2, in which the mice were put into a new cage containing only bedding material, was used in some cases. The pharmacological stimulation with ICV isoproterenol was performed in the global HSL KO mice to test whether the potential effect on food intake was due to β-adrenergic signaling or another component of the stress response.

3.3. The anorexic effect of acute stress was blunted in the whole-body HSL KO mice

Because acute inhibition of central HSL activity increased food intake, we used global HSL KO mice to study homeostatic feeding behavior. In addition to the standard genotyping, the knockout was verified on the protein level by western blotting using an antibody detecting total HSL (Supp. Figure 2A). As previously shown [43], the HSL KO mice exhibited normal food intake and a normal metabolic phenotype under basal conditions (Supp. Figure 2B). However, when exposed to injection and novelty stress, the HSL KO mice exhibited increased food intake during the 2-h period following injection stress (60% increase, Figure 3A) and for the first 12 h following novelty stress (80% increase, Figure 3B) compared to the wild-type littermates, indicating that the normal anorexic response to acute stress was blunted in the HSL KO mice. In addition, food intake in the HSL KO mice increased by 20% after 24 h of fasting (Figure 3C), a condition also characterized by high circulating levels of stress hormones, adrenaline, and noradrenaline. Concomitantly, following the 24-h fast, a pronounced increase in the expression of the orexigenic hypothalamic neuropeptides NPY and AgRP was observed in the HSL KO mice vs the littermate control mice (Figure 3D and Supp. Figure 2C).

As the decreased food intake induced by ICV administration of isoproterenol (Figure 2B) could have been due to the activation of several intracellular pathways, we specifically tested if HSL was involved in this effect using the HSL KO mice. In the mice fed a chow diet, we found that the anorexic effect of isoproterenol was completely ablated in the HSL KO mice (Figure 3E,F), indicating that HSL was crucial for the β-adrenergic signaling pathway-mediated anorexic effect, though we could not determine the cell population involved.

3.4. Increased stress-induced food intake in the HSL KO mice was reversed upon hypothalamic overexpression of HSL

To investigate whether changes in food intake are specific to HSL activity in the brain, we restored HSL expression in the mediobasal hypothalamic neurons by adeno-associated virus (AAV)-mediated overexpression under a neuron-specific promoter (Figure 4A). After the study, the mediobasal nuclei of the hypothalamus, Arc, and VMH of the AAV-injected HSL KO mice were isolated by laser-captured microdissection to confirm the overexpression of HSL using qPCR. Analysis of HSL mRNA (*Lipe*) levels revealed a 100- and 200-fold elevation compared to the control vector-treated mice in the Arc and VMH, respectively (Figure 4B). To further evaluate the distribution of the viral infusion, we administered control AAV-GFP to a separate small cohort of mice. The distribution of GFP expression confirmed the high expression in the VMH but a lower expression in the Arc. Additionally, possibly due to a high virus load, the expression in other hypothalamic regions such as the dorsomedial hypothalamus was also observed (Supp. Figure 3). AAV-mediated HSL overexpression in the hypothalamus blunted the increased food intake observed in the HSL KO mice upon exposure to injection stress (Figure 4C) and reduced the levels of *Npy* and *Agrp* mRNA in the Arc (Figure 4D). The finding that the increased stress-induced food intake observed in the global HSL KO mice could have been normalized by specific overexpression of HSL in the hypothalamus argues for a central role of HSL in the mediobasal hypothalamus as a feeding regulator during stressed conditions, but other regions may also play a role.

3.5. Brain-specific HSL deletion resulted in increased stress-induced food intake

To further delineate the role of centrally expressed HSL in regulating food intake, we inactivated HSL in the brain by crossing HSL-floxed mice with mice expressing the Cre recombinase under the control of the Nestin promoter. This strategy was chosen because Nestin-controlled Cre expression deletes target genes not only in neurons, but also in other cell types of the brain including astrocytes, where HSL is also expressed (Figure 1B and Supp. Figure 1A). Gene deletion in both neurons and astrocytes may have importance since both cell types affect lipid-mediated appetite regulation [10,14]. To control for the well-known effects of Nestin-Cre expression [23] on energy homeostasis, we compared the phenotype of the $HSL^{fl/fl}$;$cre^{+/-}$ mice (herein referred to as $HSL^{brain}KO$) with that of the $HSL^{wt/wt}$;$cre^{+/-}$ control mice (Figure 5A).

Nestin-driven Cre expression in the floxed HSL mice resulted in the absence of the enzyme in the entire brain, but not in other tissues, including adipose tissue or muscle as verified by western blotting analysis (Figure 5B). On a normal chow diet, 10- to 12-week-old $HSL^{brain}KO$ and control mice exhibited similar body weight, lean and fat mass, food intake, energy expenditure, and locomotor activity (Figure 5C–F). However, when the mice were exposed to injection stress, the $HSL^{brain}KO$ mice had a 31% higher food intake during the first 2 h after injection than the controls (Figure 5G), consistent with what was observed in the global HSL KO mice (Figures 3A and 4C), confirming that HSL in the brain regulates food intake after acute stress.

3.6. Brain-specific HSL deletion resulted in chronic hyperphagia and increased fat mass with HFD challenge

When challenged with a HFD, the $HSL^{brain}KO$ mice gained more weight than the controls (Figure 6A), which was due to a more pronounced gain of fat mass (Figure 6B) and a minor increase in lean mass (Figure 6C). The increased weight gain in the $HSL^{brain}KO$ mice was associated with increased food intake during the entire observation period (Figure 6D). Throughout the 16 weeks, the difference in total food intake was 20 g corresponding to 95 kcal ($p > 0.01$). In a subset of mice, energy expenditure and activity were assessed in calorimetry cages for the first 6 weeks of HFD feeding. During this period, the energy expenditure was slightly higher in the $HSL^{brain}KO$ mice compared to the control mice during the dark (Figure 6E, solid line) and light phases (Figure 6E, dotted line), which may have been explained by the corresponding higher body weight and lean body mass as demonstrated when expressing energy expenditure relative to both the

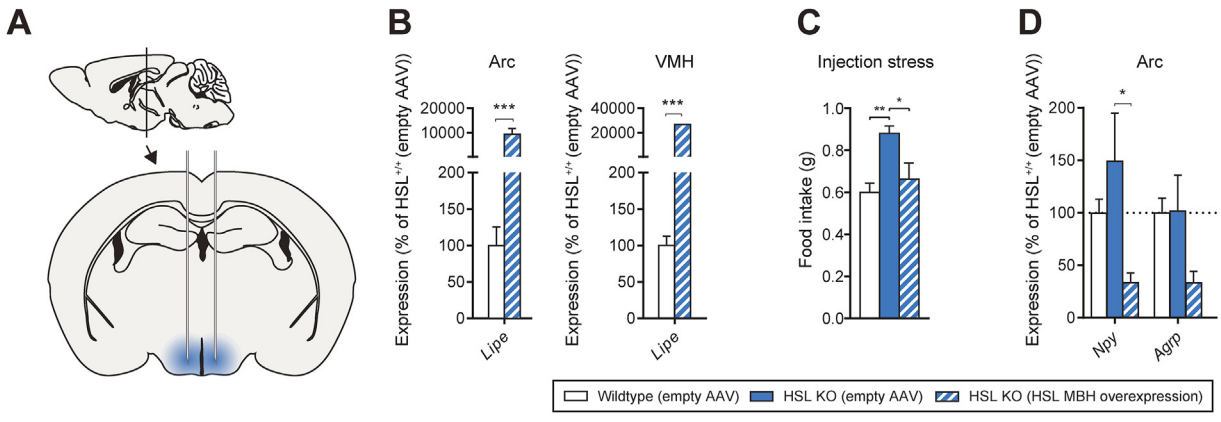

Figure 4: Food intake after stress in wild-type, HSL KO, and HSL KO mice with mediobasal hypothalamic (MBH) overexpression of HSL. A) Graphic representation of hypothalamic HSL overexpression. B) HSL expression in laser-captured microdissected Arc and VMH. C) Food intake after injection stress and D) gene expression in laser-captured microdissected Arc in wild-type, HSL KO control, and HSL KO mice with hypothalamic overexpression of HSL by AAV. Data are mean ± SEM (n = 12). *$p < 0.05$, **$p < 0.01$, and ***$p < 0.001$ based on Student's unpaired t test (B) or one-way analysis of variance followed by Tukey's multiple comparisons test (C and D).

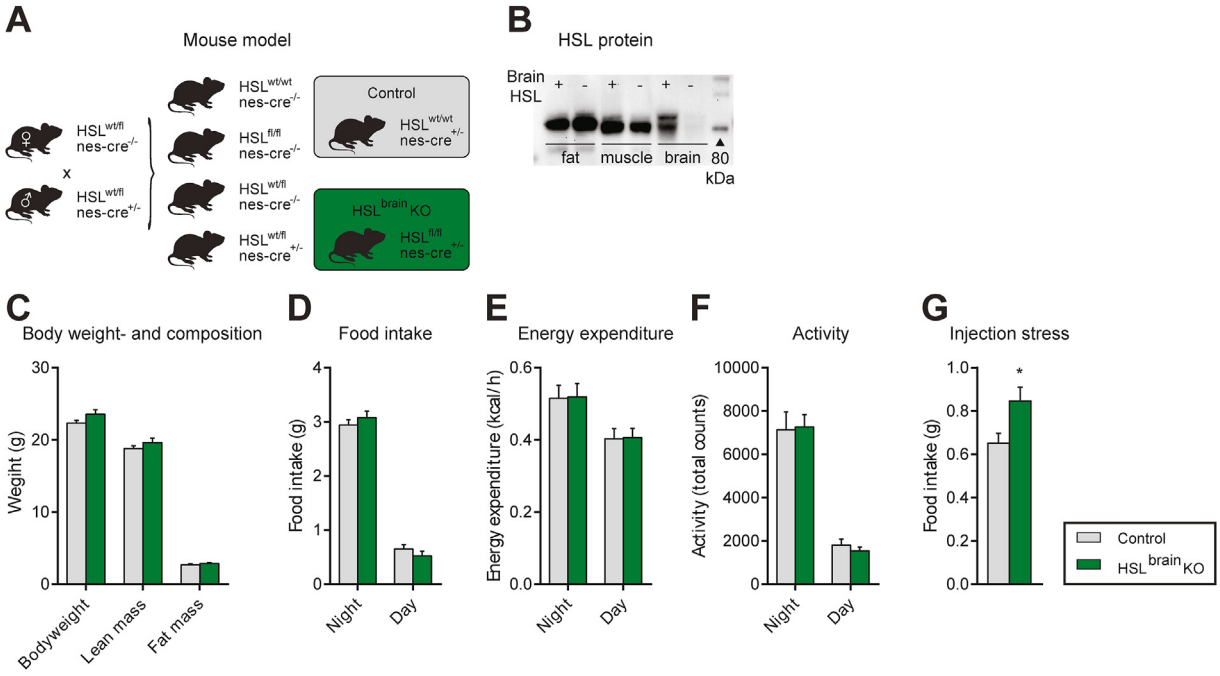

Figure 5: Metabolic phenotype of HSL^{brain}KO mice and littermate controls. A) Breeding scheme used to generate HSL^{brain}KO mice and appropriate controls. B) Western blotting verification of central but not peripheral HSL KO using a specific antibody for total HSL. C) Body weight and composition, D) food intake, E) energy expenditure, F) locomotor activity, and G) food intake after injection stress in 8- to 10-week-old HSL^{brain}KO mice and littermate controls on normal chow (n = 5–7). Data are mean ± SEM. *p < 0.05 based on Student's unpaired t test (G). No statistically significant differences for C–F based on a two-way analysis of variance.

total mass and lean mass for each investigated time point (Supp. Figure 4A). The locomotor activity was similar in the two groups (Figure 6F).

After 16 weeks of HFD feeding, an analysis of the hypothalamic gene expression showed an increased expression of *Npy* (Figure 6G) in the ad libitum fed HSL^{brain}KO mice. HSL deficiency did not result in an upregulation of hypothalamic gene expression of ATGL (*pnpla2*) or MGL (*mgll*) or the expression of other genes involved in lipid metabolism (Supp. Figure 4B). Despite the higher fat mass, there was no evidence of increased hypothalamic inflammation or decreased expression of the two anorexigenic genes thyrotropin-releasing hormone (TRH) and corticotropin-releasing hormone (CRH) in the HSL^{brain}KO mice compared to that in the controls (Supp. Figure 4B).

3.7. HSL deficiency altered lipid levels and composition

To study the substrate or product of HSL that could be responsible for the observed effects on food intake, the concentration and composition of lipid species (triacylglycerol [TAG], diacylglycerol [DAG], and fatty acids) in the mediobasal hypothalamus was measured by lipidomics analysis in samples from the HSL^{brain}KO mice fasted for 16 h [44] (Supp. Figure 5). In the HSL^{brain}KO mice, there was a trend toward increased levels of the most common TAG species (Supp. Figure 5B), but due to large variations, no significant differences were observed. Most of the DAG were detected only at a very low level (Supp. Figure 5C). However, one of the most abundant DAG species DAG36:4 was increased, and a trend ($p = 0.10$) was observed for DAG38:4 (Figure 6H,I).

3.8. The effects of central HSL deficiency on food intake were not mediated by HSL in NPY/AgRP neurons

As the increased food intake in the HSL KO and HSL^{brain}KO mice was accompanied by an increased expression of *Npy*, we hypothesized that *Npy*/*Agrp* co-expressing neurons of the Arc were responsible for the orexigenic effect of central HSL deletion. In a dataset published by Henry et al. [45] (GEO accession number GSE68177), we searched for HSL expression in AgRP neurons and found that it was significantly downregulated upon fasting (Supp. Figure 6). AgRP neurons have been shown to respond to adrenergic signaling, suggesting a modulation during stress exposure [46]. To investigate the role of HSL in AgRP neurons, we generated a mouse lacking HSL specifically in *Agrp*-positive neurons (HSL^{Agrp}KO) and induced a HFD challenge. In contrast to the HSL^{brain}KO mice, no effect on food intake and weight gain was observed (Supp. Figure 7). Therefore, we conclude that the HSL-based phenotype was not mediated by AgRP neurons and the previously observed effects on the expression of *Npy* and *Agrp* were likely indirect effects from another cell population.

3.9. Sf1 neuron-specific HSL deficiency increased stress-induced food intake and obesity during HFD challenge

As the effect on food intake in the global HSL KO mice could be reversed by overexpressing HSL in neurons of the mediobasal hypothalamus and AgRP-positive neurons did not appear to mediate the effect, we focused our attention to another mediobasal hypothalamic neuronal population, steroidogenic factor 1 (Sf1) cells of the VMH. This population of neurons has been proposed to play a key role in sensing fatty acids [47–49], and acute activation both by chemo- and optogenetic stimulation leads to an acute decrease in food intake [50,51]. Therefore, we specifically assessed the role of HSL in VMH Sf1 neurons and generated a mouse model lacking HSL in Sf1 neurons (Figure 7A). The specific HSL deletion in Sf1-positive neurons was verified by crossing the HSL^{Sf1}KO mice with mice that had a loxP-flanked STOP cassette preventing transcription of a red fluorescent protein (TdTomato) to allow the expression of TdTomato, specifically in Cre-expressing cells. Thus, the hypothalamus from the mice that were

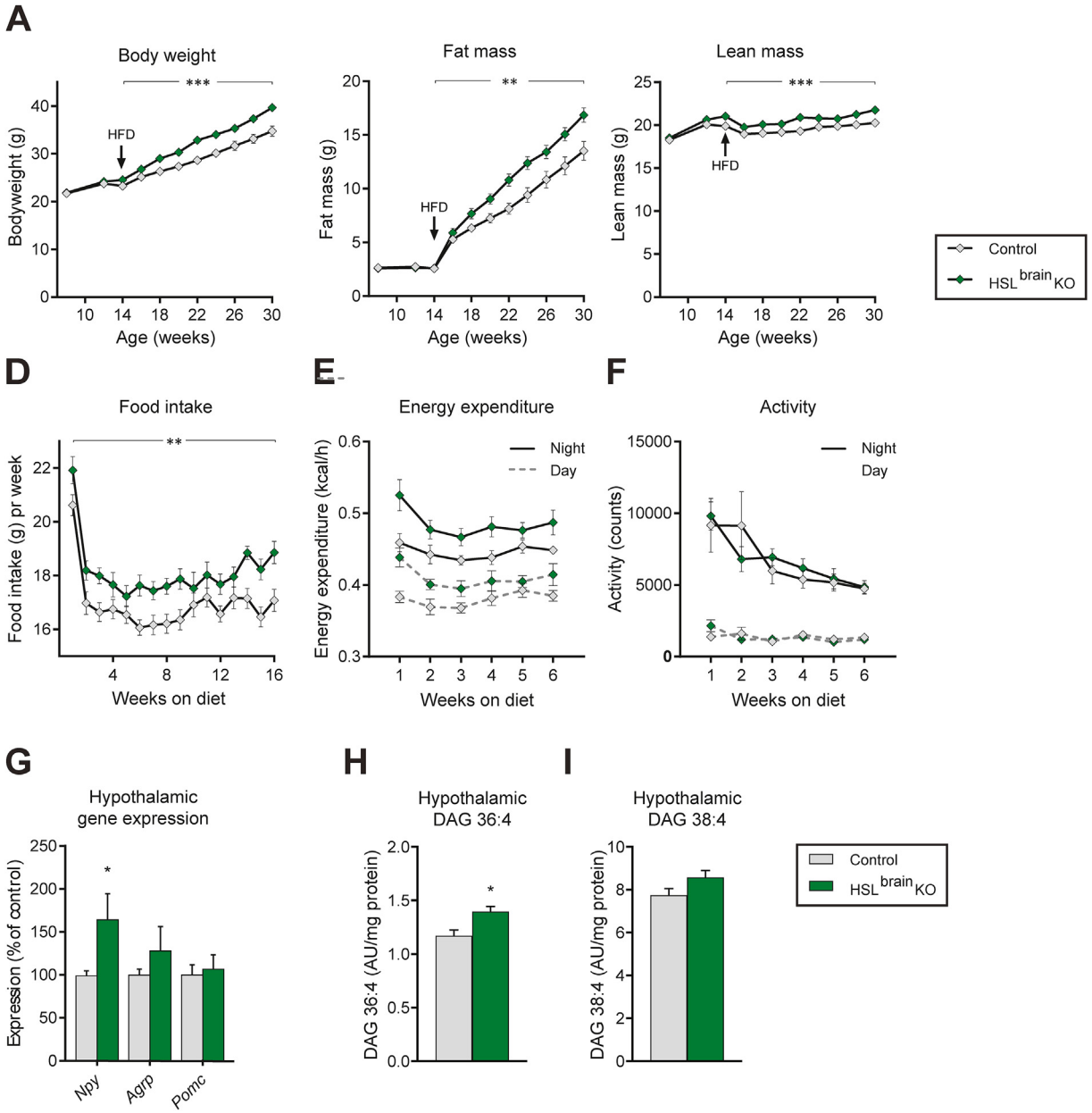

Figure 6: Metabolic phenotype of HSL^{brain}KO mice and littermate controls fed a HFD. A) Body weight, B) fat mass, and C) lean mass of HSL^{brain}KO mice and littermates switched to the HFD at 14 weeks of age (n = 9–10). D) Food intake during 16 weeks of the HFD (n = 9–10), E) energy expenditure measured for 3 days during each of the first 6 weeks of high-fat diet treatment, and F) locomotor activity during the first 6 weeks of the diet (n = 4–8). G) Hypothalamic gene expression of HSL^{brain}KO mice and littermate controls after 16 weeks of the HFD (n = 9–10). H) Relative amount of DAG36:4 and I) relative amount of DAG38:4 in the hypothalamus of HSL^{brain}KO mice and littermate controls fasted for 16 h (n = 6–9). Data are mean ± SEM. *p < 0.05, **p < 0.01, and ***p < 0.001 based on repeated measures two-way analysis of variance followed by Šídák's multiple comparisons test (A–F) or Student's unpaired t test (G, H, and I).

positive for Sf1-Cre and TdTomato and either positive or negative for HSL-flox were dissected and prepared for fluorescence-activated cell sorting (FACS) to evaluate deletion of HSL specifically in Sf1-positive cells at the mRNA level (Figure 7B).

Food intake and energy expenditure were similar in the chow-fed HSL^{Sf1}KO mice and controls (Figure 7C,D). Similarly, as observed in the HSL KO and HSL^{brain}KO mice, the HSL^{Sf1}KO mice exhibited a tendency toward increased food intake after injection stress (Figure 7E, p = 0.058), but with no difference after novelty stress or food intake after fasting (Supp. Figure 8A and 8B).

Importantly, the HSL^{Sf1}KO mice gained 30% more weight than the littermate controls after being fed an HFD (Figure 7F) primarily due to increased fat mass (Figure 7G,H). A similar degree of obesity was observed in the HSL^{Sf1}KO female mice (Supp. Figure 8C). This increase in fat mass in the HSL^{Sf1}KO mice mainly occurred during the first week of the HFD (Figure 7H, right) and was associated with increased food intake during this period (Figure 7I), with no difference in energy expenditure (Figure 7J). In a separate cohort, we observed a similar level of obesity in the HSL^{Sf1}KO mice fed a HFD diet (Supp. Figure 8D and 8E), and an oral glucose tolerance test revealed a minor degree of

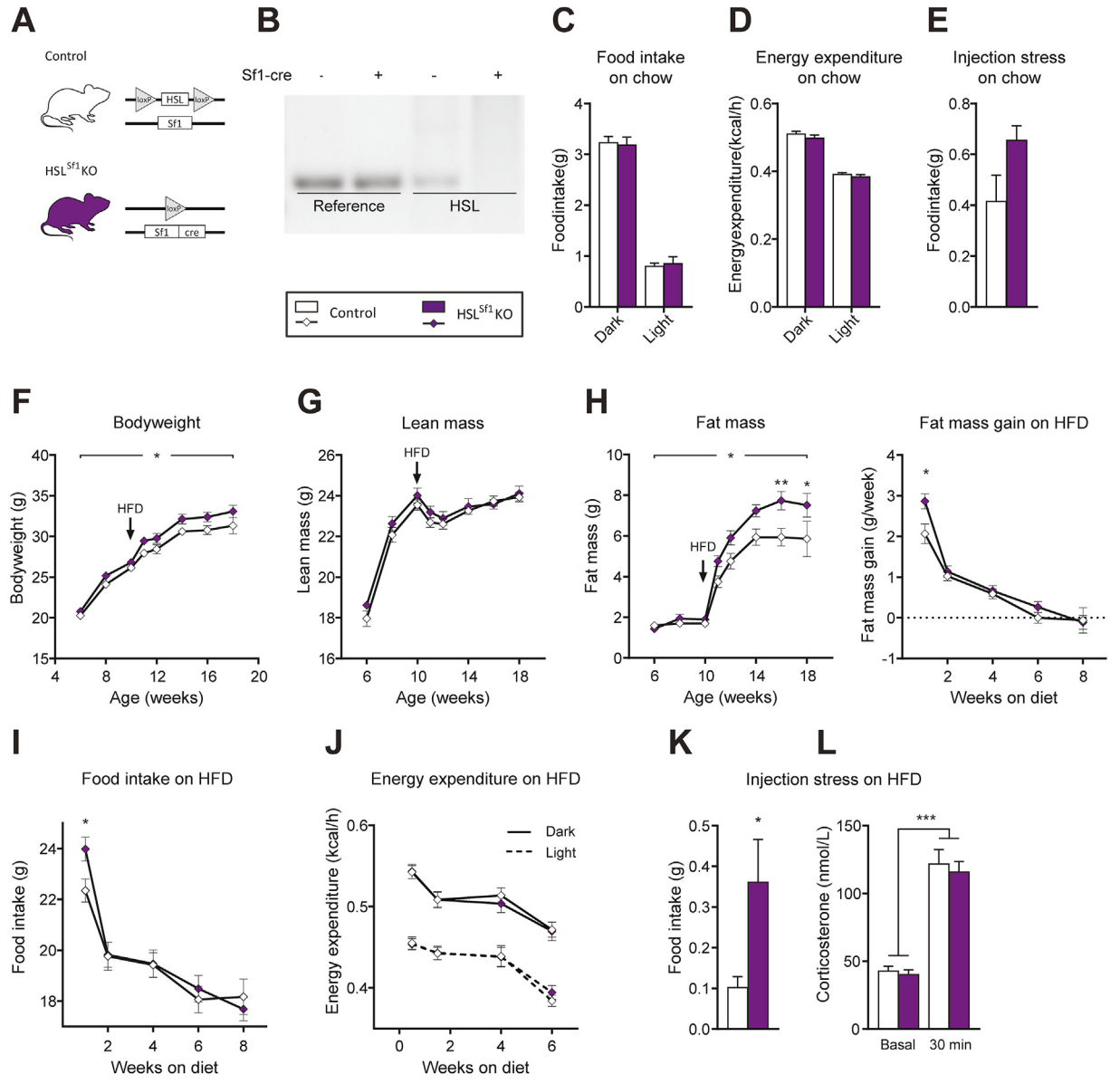

Figure 7: Metabolic phenotype of HSL^{Sf1}KO mice and littermate controls. A) Generation of HSL^{Sf1}KO mice and controls. B) Verification of HSL deletion in Sf1-positive neurons in mice expressing the Cre transgene under the Sf1 promoter but not in Cre-negative mice. C) Food intake, D) energy expenditure, and E) food intake after injection stress in 8-week-old HSL^{Sf1}KO mice and littermates on chow (n = 8). F) Body weight, G) lean mass, and H) fat mass of HSL^{Sf1}KO mice and littermates switched to a HFD at 10 weeks of age (n = 8). I) Food intake and J) energy expenditure during 6 weeks of HFD in HSL^{Sf1}KO mice and littermates (n = 8). K) Food intake after injection stress in HSL^{Sf1}KO mice and littermates fed a HFD and L) verification of stress response 30 min after injection stress in the same mice (n = 8) by measuring plasma corticosterone. Data are mean ± SEM. *p < 0.05, **p < 0.01, and ***p < 0.001 based on repeated measures two-way analysis of variance followed by Šídák's multiple comparisons test (F—J) or Student's unpaired t test (C-E and K-L).

glucose intolerance without any significant difference in insulin secretion (Supp. Figure 8F and 8G). We suggest that the obese phenotype was responsible for the increased glucose levels; however, we cannot exclude modulation of the sympathetic nervous system, as SF1 neurons have been described to affect glucose tolerance, possibly via modulation of the sympathetic nervous system [52].

With the HFD challenge, the HSL^{Sf1}KO mice exhibited a significant increase in food intake when exposed to injection stress (Figure 7K). To verify the stress response, the plasma corticosterone concentration was assessed under pre-stress exposure and 30 min after stress exposure. Upon stress exposure, corticosterone concentrations increased in the control and HSL^{Sf1}KO mice to a similar extent (Figure 7L). These results suggest that HSL in Sf1-positive neurons plays a role in mediating the stress-induced increase in food intake independent of the corticosterone level and that HSL contributes to energy homeostasis during HFD conditions.

4. DISCUSSION

The present study investigated the importance of central HSL expression in the regulation of food intake and body weight in mice to clarify whether intracellular lipolysis in the mammalian hypothalamus plays a role in regulating appetite. We found that HSL was expressed in hypothalamic nuclei known to be important for appetite regulation.

Hypothalamic HSL was activated by isoproterenol in vitro and stress in vivo, indicating regulation similar to that in the periphery. In vivo, we found that pharmacological inhibition of central HSL acutely increased food intake and the global HSL KO mice had blunted stress-induced reductions in food intake, a phenotype that can be reversed by overexpression of HSL in the hypothalamus. This increased food intake after stress was also present in the HSL^{brain}KO and HSL^{Sf1}KO mice. Central HSL deficiency caused higher sustained food intake when the mice were fed a high-fat diet, resulting in significantly increased body weight gain primarily due to increased fat mass. The HSL^{Sf1}KO mice also displayed a transient increase in food intake after being switched to an HFD, which resulted in increased body weight. As food intake was not significantly higher under basal conditions in the HSL^{brain}KO and HSL^{Sf1}KO mice when fed a standard chow diet, this result suggested that in addition to contributing to stress-induced hypophagia, HSL also plays an important role in the central nervous system in sensing the caloric content or fat in the diet.

It is known that acute stress and β-adrenergic signaling decrease food intake, and from an evolutionary perspective, decreased food intake is an advantage when the body is in a stressful "fight-or-flight" situation [53]. Here we showed for the first time that HSL in the brain is important for the centrally mediated part of this hypophagic response to acute stress. ICV administration of isoproterenol was used as a pharmacological model imitating the β-adrenergic part of the acute stress response, and strongly decreased food intake in the wild-type mice, but the response was completely abolished in the HSL KO mice. The acute stress response is complex and involves several different hormones and neuronal axes, of which corticotropin-releasing hormone (CRH), as part of the hypothalamic-pituitary-adrenal axis, is one of the best-described hormones. Importantly, CRH plays a major role in appetite regulation as it is an anorexigenic transmitter in the paraventricular nucleus, where noradrenergic projections activate CRH neurons and vice versa [53]. We did not see a differential regulation of CRH at the mRNA level in the hypothalamus from the HSL^{brain}KO compared to the wild-type mice, but we cannot exclude involvement of the CRH system in the food intake phenotype observed with HSL deficiency. Under physiological conditions, different adrenergic receptors have been described to participate in stress-induced hypophagia [54,55]; however, in the present study, we characterized only hypophagia induced by β-adrenergic activation and demonstrated that it was completely abolished by the absence of HSL.

To elucidate the downstream mechanisms underlying the appetite phenotype in the HSL-deficient mice, we performed a lipidomic analysis of the hypothalamus of the fasted HSL^{brain}KO mice. As fatty acids have previously been shown to decrease food intake [4,9], and as fatty acid released from brain extracts has been shown to be significantly decreased in HSL KO mice [19], we hypothesized that decreased levels of fatty acids were driving the hyperphagic phenotype of the HSL^{brain}KO mice. In our study, we did not observe overall changes in fatty acid concentrations in the mediobasal hypothalamus (Supp. Figure 4). However, given our whole-tissue fatty acid quantification methodology, any localized or cell-specific paracrine effects on fatty acid metabolism that could regulate food intake may have been obscured.

Only one species of diacylglycerol, DAG36:4, was slightly increased in the mediobasal hypothalamus and may have contributed to the effects on food intake. In this respect, it is interesting that ICV administration of conjugated linolenic acid, which is a molecule similar to DAG36:4 as it consists of two linolenate (18:2) chains bound to a glycerol backbone, has been shown to decrease both food intake and the expression of NPY and AgRP [56]. Of note, diacylglycerol can be derived from sources other than lipolysis, which may influence its ability to act as a signaling molecule [57], and it has been shown that ATGL preferentially hydrolyzes TAG in the sn-2 position, producing primarily sn-1,3 DAG. The current analysis did not distinguish between the different pools of diacylglycerol molecules [57,58], and unchanged pools of sn-1,2 DAG may have concealed the relative difference in sn-1,3 DAG. The hypothesis that diacylglycerols mediate the observed effects on food intake is supported by the fact that ATGL KO mice are resistant to diet-induced weight gain as a result of decreased food intake [59]. In contrast, global HSL KO mice are resistant to diet-induced obesity despite increased food intake [60]. While HSL executes the second step of lipolysis, ATGL predominantly catalyzes the first step and therefore it is possible that elevated levels of diacylglycerol increase food intake. Accordingly, diacylglycerol levels were reduced in the ATGL KO mice but elevated in the HSL KO mice vs controls and therefore may mediate decreased or increased appetite, respectively. In addition to a role in mediating stress-induced hypophagia, our data suggest that HSL plays a role in the central nervous system in sensing dietary fat content since central HSL deficiency caused sustained increased food intake when the mice were fed a HFD, resulting in increased body weight gain primarily due to increased fat mass. Sf-1-positive neurons have previously been described to modulate energy homeostasis primarily by changes in energy expenditure during a HFD [61,62]. Our data from the HSL^{brain}KO mice indicated that a lack of HSL in the brain increased susceptibility to HFD with increased body weight gain and fat accumulation and that this effect to some degree could be attributed to HSL in Sf1-positive neurons. In contrast to other genes expressed in Sf1 neurons, such as leptin and estrogen receptors, HSL deficiency in these neurons appears to affect food intake more strongly than energy expenditure, although we cannot exclude modulation of energy expenditure [62,63].

The hyperphagic and obese phenotypes displayed by the HFD-fed HSL^{brain}KO and HSL^{Sf1}KO mice contrasts the phenotype of the global HSL KO mice and HSL-deficient humans, wherein both suffer from lipodystrohy [19,43,64] and are resistant to obesity when fed a HFD [43,60]. This counterintuitive inability to store fat in the absence of HSL has been shown to result from a concomitant reduction in adipogenic activity [60], such as defective peroxisome proliferator-activated receptor-γ (PPARγ) signaling [19,64,65]. In fact, global HSL KO mice are leaner despite increased food intake per gram of body weight [60]. In addition, this obesity-resistant phenotype in global HSL KO mice is due to increased energy expenditure. Hence, while these results may appear conflicting, they instead underscore that the peripheral expression of HSL exerts effects on energy expenditure and fat accumulation that differ from the effects mediated by centrally expressed HSL. In particular, the obesity-prone phenotype observed in the HSL^{brain}KO mice and to some degree in the HSL^{Sf1}KO mice highlights that the function of HSL in the brain markedly differs from the function in the peripheral tissues.

The specific cell types responsible for HSL-mediated hypophagia are not entirely clear, but the finding that reduced hypophagia after acute stress in the global HSL KO mice could be normalized by specific overexpression of HSL in the mediobasal hypothalamus under a neuron-specific promotor argues for a role of HSL in this region of the hypothalamus. As the RNA analysis of the hypothalamus from the HSL KO and HSL^{brain}KO mice showed increased expression of *Npy*, we investigated the role of HSL in these neurons. However, we did not see the same effect on food intake and obesity development in the HSL^{Agrp}KO mice, suggesting that the phenotype was not directly mediated by this neuronal population. In contrast, we observed significantly higher food intake after exposure to injection stress in the HSL^{Sf1}KO mice after the HFD and a trend toward increased food intake even in the lean HSL^{Sf1}KO

mice. This suggests that HSL activation in Sf1 neurons of the VMH may play a role in the hypophagic response to stress induced by injection. As Sf1 neurons have been demonstrated to form excitatory projections to the anorexigenic POMC neurons of the Arc, it could be speculated that a lack of HSL weakens these projections and hence results in increased hunger [66]. However, although the HFD-fed HSL^{Sf1} mice exhibited acute blunted hypophagia, the effect was less pronounced in comparison with the HFD-fed $HSL^{brain}KO$ mice. This suggests that HSL in other cell types or areas of the brain may be involved in the HSL-mediated modulation of food intake, possibly through a different mechanism not involving β-adrenergic signaling.

5. CONCLUSION

In summary, we showed for the first time that central HSL deficiency has effects on food intake and energy homeostasis through its function in the mediobasal hypothalamus. We demonstrated that HSL in the hypothalamus appears to be regulated in a similar manner as in the periphery via the activation of β-adrenergic receptor signaling, and that without functional HSL, the decrease in food intake induced by acute stress is blunted. In addition, lack of central HSL increases susceptibility to HFD, suggesting a role in sensing fat and modulating energy homeostasis according to surplus energy. Collectively, these results demonstrate an important role of the central expression of HSL in regulating food intake and maintaining energy balance.

AUTHOR CONTRIBUTIONS

Experiments with the mouse characterization of HSL wild-type and knockout models were designed by CH, RZ, DP, BK, and BH and conducted and analyzed by CH, PK, HBB, LJS, SHC, LT, AWH, MPM, CR, AKS, JJT, THP, DDW, and BH. Experiments with lipids in the hypothalamus were designed by CH, PK, DP, RZ, BK, and BH and performed and analyzed by CH, PK, and DP. CH, RZ, DP, BK, LJS, and BH interpreted the overall results. CH, RZ, BK, LJS, and BH drafted the manuscript. All the authors edited, revised, and approved the final manuscript.

ACKNOWLEDGEMENTS

We thank Dr. Alessandra Misto for help with lipid analyses and Christian Fledelius at Novo Nordisk for providing the HSL inhibitor. This work was supported by a Project grants in Endocrinology and Metabolism - Nordic Region 2019 (#0057417) and by a The Novo Nordisk Foundation Center for Basic Metabolic Research (www.metabol.ku.dk), which is supported by an unconditional grant (NNF10CC1016515) from the Novo Nordisk Foundation to University of Copenhagen.

CONFLICT OF INTEREST

None declared.

APPENDIX A. SUPPLEMENTARY DATA

Supplementary data to this article can be found online at https://doi.org/10.1016/j.molmet.2021.101174.

REFERENCES

[1] Sinha, R., 2018. Role of addiction and stress neurobiology on food intake and obesity. Biological Psychology 131:5–13.

[2] Rasmussen, B.A., Breen, D.M., Lam, T.K.T., 2012. Lipid sensing in the gut, brain and liver. Trends in Endocrinology and Metabolism 23:49–55.

[3] Oomura, Y., Nakamura, T., Sugimori, M., Yamada, Y., 1975. Effect of free fatty acid on the rat lateral hypothalamic neurons. Physiology & Behavior 14: 483–486.

[4] Obici, S., Feng, Z., Morgan, K., Stein, D., Karkanias, G., Rossetti, L., 2002. Central administration of oleic acid inhibits glucose production and food intake. Diabetes 51:271–275.

[5] Blouet, C., Schwartz, G.J., 2010. Hypothalamic nutrient sensing in the control of energy homeostasis. Behavioural Brain Research 209:1–12.

[6] Cota, D., Proulx, K., Seeley, R.J., 2007. The role of CNS fuel sensing in energy and glucose regulation. Gastroenterology 132:2158–2168.

[7] Moullé, V.S., Picard, A., Le Foll, C., Levin, B.E., Magnan, C., 2014. Lipid sensing in the brain and regulation of energy balance. Diabetes & Metabolism 40:29–33.

[8] Lam, T.K.T., Schwartz, G.J., Rossetti, L., 2005. Hypothalamic sensing of fatty acids. Nature Neuroscience 8:579–584.

[9] Morgan, K., Obici, S., Rossetti, L., 2004. Hypothalamic responses to long-chain fatty acids are nutritionally regulated. Journal of Biological Chemistry 279:31139–31148.

[10] Wang, H., Astarita, G., Taussig, M.D., Bharadwaj, K.G., Dipatrizio, N.V., Nave, K.A., et al., 2011. Deficiency of lipoprotein lipase in neurons modifies the regulation of energy balance and leads to obesity. Cell Metabolism 13: 105–113.

[11] Laperrousaz, V.S., Moullé, R.G., Denis, N., Kassis, C., Berland, B., Colsch, E., et al., 2017. Lipoprotein lipase in hypothalamus is a key regulator of body weight gain and glucose homeostasis in mice. Diabetologia 60:1314–1324.

[12] Picard, A., Rouch, C., Kassis, N., Moullé, V.S., Croizier, S., Denis, R.G., et al., 2014. Hippocampal lipoprotein lipase regulates energy balance in rodents. Molecular Metabolism 3:167–176.

[13] Wang, H., Taussig, M.D., Dipatrizio, N.V., Bruce, K., Piomelli, D., Eckel, R.H., 2016. Obesity development in neuron-specific lipoprotein lipase deficient mice is not responsive to increased dietary fat content or change in fat composition. Metabolism 65:987–997.

[14] Gao, Y., Layritz, C., Legutko, B., Eichmann, T.O., Laperrousaz, E., Moullé, V.S., et al., 2017. Disruption of lipid uptake in astroglia exacerbates diet induced obesity. Diabetes 66:db161278.

[15] Zechner, R., Madeo, F., Kratky, D., 2017. Cytosolic lipolysis and lipophagy: two sides of the same coin. Nature Reviews Molecular Cell Biology 18:671–684.

[16] Lafontan, M., Langin, D., 2009. Lipolysis and lipid mobilization in human adipose tissue. Progress in Lipid Research 48:275–297.

[17] Hofer, P., Taschler, U., Schreiber, R., Kotzbeck, P., Schoiswohl, G., 2020. The lipolysome—a highly complex and dynamic protein network orchestrating cytoplasmic triacylglycerol degradation. Metabolites 10:1–27.

[18] Mergenthaler, P., Lindauer, U., Dienel, G.A., Meisel, A., 2013. Sugar for the brain: the role of glucose in physiological and pathological brain function. Trends in Neurosciences 36:587–597.

[19] Haemmerle, G., Zimmermann, R., Hayn, M., Theussl, C., Waeg, G., Wagner, E., et al., 2002. Hormone-sensitive lipase deficiency in mice causes diglyceride accumulation in adipose tissue, muscle, and testis. Journal of Biological Chemistry 277:4806–4815.

[20] Mulder, H., Sörhede-Winzell, M., Contreras, J.A., Fex, M., Ström, K., Ploug, T., et al., 2003. Hormone-sensitive lipase null mice exhibit signs of impaired insulin sensitivity whereas insulin secretion is intact. Journal of Biological Chemistry 278:36380–36388.

[21] Grober, J., Lucas, S., Sörhede-Winzell, M., Zaghini, I., Mairal, A., Contreras, J.A., et al., 2003. Hormone-sensitive lipase is a cholesterol esterase of the intestinal mucosa. Journal of Biological Chemistry 278:6510–6515.

[22] Tronche, F., Kellendonk, C., Kretz, O., Gass, P., Anlag, K., Orban, P.C., et al., 1999. Disruption of the glucocorticoid receptor gene in the nervous system results in reduced anxiety. Nature Genetics 23:99–103.

[23] Harno, E., Cottrell, E.C., White, A., 2013. Metabolic pitfalls of CNS cre-based technology. Cell Metabolism, 18 21—28.
[24] Franklin, K.B.J., Paxinos, G., 2001. The mouse brain in stereotaxic coordinates.
[25] Christensen, D.Z., Olesen, M.V., Kristiansen, H., Mikkelsen, J.D., Woldbye, D.P.D., 2006. Unaltered neuropeptide Y (NPY) - stimulated [35 S] GTP g S binding suggests a net increase in NPY signalling after repeated electroconvulsive seizures in mice 1291:1282—1291.
[26] Woldbye, D.P.D., Nanobashvili, A., Sørensen, A.V., Husum, H., Bolwig, T.G., Sørensen, G., et al., 2005. Differential suppression of seizures via Y2 and Y5 neuropeptide Y receptors. Neurobiology of Disease 20:760—772.
[27] Macosko, E.Z., Basu, A., Satija, R., Nemesh, J., Shekhar, K., Goldman, M., et al., 2015. Highly parallel genome-wide expression profiling of individual cells using nanoliter droplets. Cell 161:1202—1214.
[28] Campbell, J.N., Macosko, E.Z., Fenselau, H., Pers, T.H., Lyubetskaya, A., Tenen, D., et al., 2017. A molecular census of arcuate hypothalamus and median eminence cell types. Nature Neuroscience 20:484—496.
[29] Stuart, T., Butler, A., Hoffman, P., Hafemeister, C., Papalexi, E., Mauck, W.M., et al., 2019. Comprehensive integration of single-cell data. Cell 177:1888—1902 e21.
[30] Venables, W.N., Ripley, B.D., 2002. Modern applied statistics with S. Springer.
[31] Wickham, H., 2016. Elegant graphics for data analysis. Springer-Verlag New York.
[32] Dhillon, S.S., McFadden, S.A., Chalmers, J.A., Centeno, M.L., Kim, G.L., Belsham, D.D., 2011. Cellular leptin resistance impairs the leptin-mediated suppression of neuropeptide Y secretion in hypothalamic neurons. Endocrinology 152:4138—4147.
[33] Matyash, V., Liebisch, G., Kurzchalia, T.V., Shevchenko, A., Schwudke, D., 2008. Lipid extraction by methyl-terf-butyl ether for high-throughput lipidomics. The Journal of Lipid Research 49:1137—1146.
[34] Holm, C., Osterlund, T., Laurell, H., Contreras, J.a., 2003. Molecular mechanisms regulating hormone-sensitive lipase and lipolysis. Biochemical Society Transactions 20:1120—1124.
[35] Maniam, J., Morris, M.J., 2012. The link between stress and feeding behaviour. Neuropharmacology 63:97—110.
[36] Calvez, J., Fromentin, G., Nadkarni, N., Darcal, N., Even, P., Tom, D., et al., 2011. Inhibition of food intake induced by acute stress in rats is due to satiation effects. Physiology & Behavior 104:675—683.
[37] Martí, O., Martí, J., Armario, a., 1994. Effects of chronic stress on food intake in rats: influence of stressor intensity and duration of daily exposure. Physiology & Behavior 55:747—753.
[38] Pecoraro, N., Reyes, F., Gomez, F., Bhargava, A., Dallman, M.F., 2004. Chronic stress promotes palatable feeding, which reduces signs of stress: feedforward and feedback effects of chronic stress. Endocrinology 145:3754—3762.
[39] Meijer, M.K., Spruijt, B.M., van Zutphen, L.F.M., Baumans, V., 2006. Effect of restraint and injection methods on heart rate and body temperature in mice. Lab Animal 40:382—391.
[40] Saegusa, Y., Takeda, H., Muto, S., Nakagawa, K., Ohnishi, S., Sadakane, C., et al., 2011. Decreased plasma ghrelin contributes to anorexia following novelty stress. AJP Endocrinology Metabolism 301:E685—E696.
[41] Kaur, R., Jaggi, A.S., Singh, N., 2010. Studies on effect of stress preconditioning in restrain stress-induced behavioral alterations. Yakugaku Zasshi 130:215—221.
[42] Galliot, E., Laurent, L., Hacquemand, R., Pourié, G., Millot, J.L., 2012. Fear-like behavioral responses in mice in different odorant environments: trigeminal versus olfactory mediation under low doses. Behavioural Processes 90:161—166.
[43] Osuga, J., Ishibashi, S., Oka, T., Yagyu, H., Tozawa, R., Fujimoto, A., et al., 2000. Targeted disruption of hormone-sensitive lipase results in male sterility and adipocyte hypertrophy, but not in obesity. Proceedings of the National Academy of Sciences of the United States of America 97:787—792.
[44] Husted, A.S., Trauelsen, M., Rudenko, O., Hjorth, S.A., Schwartz, T.W., 2017. GPCR-mediated signaling of metabolites. Cell Metabolism 25:777—796.
[45] Henry, F.E., Sugino, K., Tozer, A., Branco, T., Sternson, S.M., 2015. Cell type-specific transcriptomics of hypothalamic energy-sensing neuron responses to weight-loss. Elife 4.
[46] Paeger, L., Karakasilioti, I., Altmüller, J., Frommolt, P., Brüning, J., Kloppenburg, P., 2017. Antagonistic modulation of NPY/AgRP and POMC neurons in the arcuate nucleus by noradrenalin. Elife 6:1—18.
[47] López, M., Lelliott, C.J., Tovar, S., Kimber, W., Gallego, R., Virtue, S., et al., 2006. Tamoxifen-induced anorexia is associated with fatty acid synthase inhibition in the ventromedial nucleus of the hypothalamus and accumulation of malonyl-CoA. Diabetes 55:1327—1336.
[48] Gao, S., Zhu, G., Gao, X., Wu, D., Carrasco, P., Casals, N., et al., 2011. Important roles of brain-specific carnitine palmitoyltransferase and ceramide metabolism in leptin hypothalamic control of feeding. Proceedings of the National Academy of Sciences of the United States of America 108:9691—9696.
[49] López, M., Lage, R., Saha, A.K., Pérez-Tilve, D., Vázquez, M.J., Varela, L., et al., 2008. Hypothalamic fatty acid metabolism mediates the orexigenic action of ghrelin. Cell Metabolism 7:389—399.
[50] Viskaitis, P., Irvine, E.E., Smith, M.A., Choudhury, A.I., Alvarez-Curto, E., Glegola, J.A., et al., 2017. Modulation of SF1 neuron activity coordinately regulates both feeding behavior and associated emotional states. Cell Reports 21:3559—3572.
[51] Coutinho, E.A., Okamoto, S., Ishikawa, A.W., Yokota, S., Wada, N., Hirabayashi, T., et al., 2017. Activation of SF1 neurons in the ventromedial hypothalamus by DREADD technology increases insulin sensitivity in peripheral tissues. Diabetes 66:2372—2386.
[52] Felsted, J.A., Chien, C., Wang, D., Panessiti, M., Ameroso, S., Greenberg, A., et al., 2017. Alpha2delta-1 in SF1+ neurons of the ventromedial hypothalamus is an essential regulator of glucose and lipid homeostasis. Cell Reports 21:2737—2747.
[53] Dunn, A.J., Swiergiel, A.H., 2008. The role of corticotropin-releasing factor and noradrenaline in stress-related responses, and the inter-relationships between the two systems. European Journal of Pharmacology 583:186—193.
[54] Maniscalco, J.W., Rinaman, L., 2017. Interoceptive modulation of neuroendocrine, emotional, and hypophagic responses to stress. Physiology & Behavior 176:195—206.
[55] Boundy, V.A., Cincotta, A.H., 2000. Hypothalamic adrenergic receptor changes in the metabolic syndrome of genetically obese (ob/ob) mice. American Journal of Physiology - Regulatory, Integrative and Comparative Physiology 279.
[56] Cao, Z.-P., Wang, F., Xiang, X.-S., Cao, R., Zhang, W.-B., Gao, S.-B., 2007. Intracerebroventricular administration of conjugated linoleic acid (CLA) inhibits food intake by decreasing gene expression of NPY and AgRP. Neuroscience Letters 418:217—221.
[57] Serup, A.K., et al., 2016. Partial disruption of lipolysis increases postexercise insulin sensitivity in skeletal muscle despite accumulation of DAG. Diabetes 65:2932—2942.
[58] Petersen, M.C., Shulman, G.I., 2017. Roles of diacylglycerols and ceramides in hepatic insulin resistance. Trends in Pharmacological Sciences 38:649—665.
[59] Schreiber, R., Hofer, P., Taschler, U., Voshol, P.J., Rechberger, G.N., Kotzbeck, P., et al., 2015. Hypophagia and metabolic adaptations in mice with defective ATGL-mediated lipolysis cause resistance to HFD-induced obesity. Proceedings of the National Academy of Sciences of the United States of America 112:13850—13855.
[60] Harada, K., Shen, W.-J., Patel, S., Natu, V., Wang, J., Osuga, J., et al., 2003. Resistance to high-fat diet-induced obesity and altered expression of adipose-specific genes in HSL-deficient mice. American Journal of Physiology. Endocrinology and Metabolism 285:1182—1195.
[61] Kim, K.W., Zhao, L., Donato, J., Kohno, D., Xu, Y., Eliasa, C.F., et al., 2011. Steroidogenic factor 1 directs programs regulating diet-induced thermogenesis

and leptin action in the ventral medial hypothalamic nucleus. Proceedings of the National Academy of Sciences of the United States of America 108: 10673–10678.

[62] Choi, Y.H., Fujikawa, T., Lee, J., Reuter, A., Kim, K.W., 2013. Revisiting the ventral medial nucleus of the hypothalamus: the roles of SF-1 neurons in energy homeostasis. Frontiers in Neuroscience. https://doi.org/10.3389/fnins.2013.00071.

[63] King, B.M., 2006. The rise, fall, and resurrection of the ventromedial hypothalamus in the regulation of feeding behavior and body weight. Physiology & Behavior, 87 221–244.

[64] Albert, J.S., Yerges-Armstrong, L.M., Horenstin, R.B., Pollin, T.I., Sreenivasan, U.T., Chai, S., et al., 2014. Null mutation in hormone-sensitive lipase gene and risk of type 2 diabetes. New England Journal of Medicine 370:2307–2315.

[65] Zimmermann, R., Haemmerle, G., Wagner, E.M., Strauss, J.G., Kratky, D., Zechner, R., 2003. Decreased fatty acid esterification compensates for the reduced lipolytic activity in hormone-sensitive lipase-deficient white adipose tissue. The Journal of Lipid Research 44:2089–2099.

[66] Sternson, S.M., G Shepherd, G.M., Friedman, J.M., 2005. Topographic mapping of VMH-arcuate nucleus microcircuits and their reorganization by fasting. https://doi.org/10.1038/nn1550.

